ACS APPLIED MATERIALS & INTERFACES

www.acsami.org Research Article

Biofunctional Silk Kirigami With Engineered Properties

Sayantan Pradhan, Leonardo Ventura, Francesca Agostinacchio, Meng Xu, Ettore Barbieri, Antonella Motta, Nicola M. Pugno,* and Vamsi K. Yadavalli*

Cite This: *ACS Appl. Mater. Interfaces* 2020, 12, 12436−12444 Read Online

ACCESS | Metrics & More | Article Recommendations | Supporting Information

ABSTRACT: The fabrication of multifunctional materials that interface with living environments is a problem of great interest. A variety of structural design concepts have been integrated with functional materials to form biodevices and surfaces for health monitoring. In particular, approaches based on kirigami-inspired cuts can engineer flexibility in materials through the creation of patterned defects. Here, the fabrication of a biodegradable and biofunctional "silk kirigami" material is demonstrated. Mechanically flexible, free-standing, optically transparent, large-area biomaterial sheets with precisely defined and computationally designed microscale cuts can be formed using a single-step photolithographic process. Using modeling techniques, it is shown how cuts can generate remarkable "self-shielding" leading to engineered elastic behavior and deformation. As composites with conducting polymers, flexible, intrinsically electroactive sheets can be formed. Importantly, the silk kirigami sheets are biocompatible, can serve as substrates for cell culture, and be proteolytically resorbed. The unique properties of silk kirigami suggest a host of applications as transient, "green", functional biointerfaces, and flexible bioelectronics.

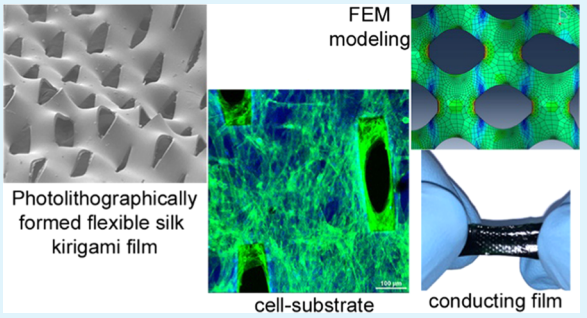

KEYWORDS: *silk fibroin, kirigami, micropatterning, conducting polymer, flexible, biodegradable*

1. INTRODUCTION

Producing flexible, thin, mechanically robust, and compliant interfaces that perform in dynamic environments is an ongoing challenge.[1,2] Such multifunctionality can establish adaptive interfaces with the body.[3] From human−machine interfaces and soft robotics, to implantable devices and engineered tissues for regenerative medicine, material design and fabrication strategies have focused on capturing the mechanical compliance and biomimetic sensing of skin.[4−6] Various architectures have been proposed to impart functional conformability with biological tissues including meshes, cracks, prestressing, buckling, and serpentine designs.[7,8] Integrating biocompatibility and biodegradation can vastly expand the scope of synthetic "skins" for applications in biohybrid systems, soft matter electronics,[9] prosthetics,[10] wound healing, neural interfaces, and health monitoring in situ.[11,12] Across length scales, micropatterned and microstructured materials may be used for cell co-cultures and spatial control.[13−15] Recently, approaches building on principles borrowed from the Japanese paper arts, such as origami and kirigami, have shown great promise.[16] Origami refers to folding ("ori-"), whereas kirigami involves cutting ("kiri-") of paper ("-gami"). Complex and functional objects using combinations of cutting, bending, and/or folding of diverse materials have been shown artistically and scientifically.[17]

Of interest is the use of kirigami-inspired cuts to transform materials toward multifunctional biointerfaces. While designed to enhance elasticity for traditionally stiff materials, kirigami architectures can transform intrinsically flexible and soft materials in interesting ways. For instance, mechanical properties at scales smaller than the cuts would not change, whereas effective properties at scales larger than the cuts would.[18] Substrates can be imbued with deformability beyond the strain limits of pristine materials, allowing for multifunctionality, e.g., stretchability, conformability to complex interfaces, conductivity, fault tolerance, biocompatibility, and reconfigurability. Out-of-plane deformations can enable reversible geometry changes, transforming between planar two dimensional (2D) and three dimensional (3D).[8,17,19] Using computational tools, it is possible to predict and thereby precisely engineer the operative behaviors under mechanical stresses.

Previously, kirigami cuts have been accomplished using subtractive methods including microscale laser cutting,[20] optical lithography,[21] etching (e.g., plasma, masked ion),[22] and macroscopic cutting (e.g., x-acto knives).[23] In addition to

Received: November 20, 2019
Accepted: February 25, 2020
Published: February 25, 2020

https://dx.doi.org/10.1021/acsami.9b20691
ACS Appl. Mater. Interfaces 2020, 12, 12436−12444

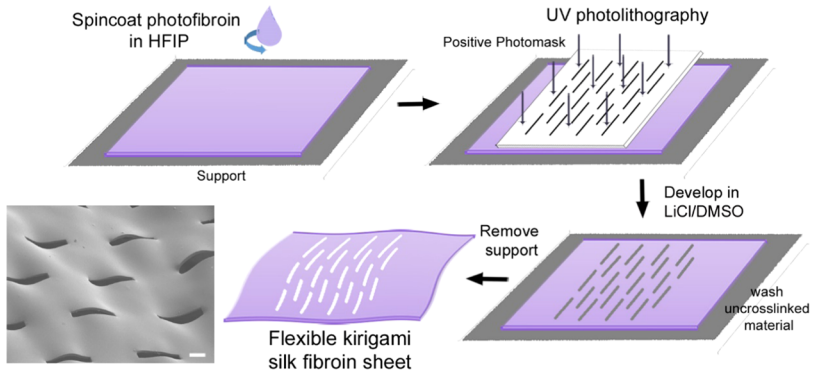

Figure 1. Schematic: single-step fabrication of kirigami cuts in silk fibroin films via photolithography.

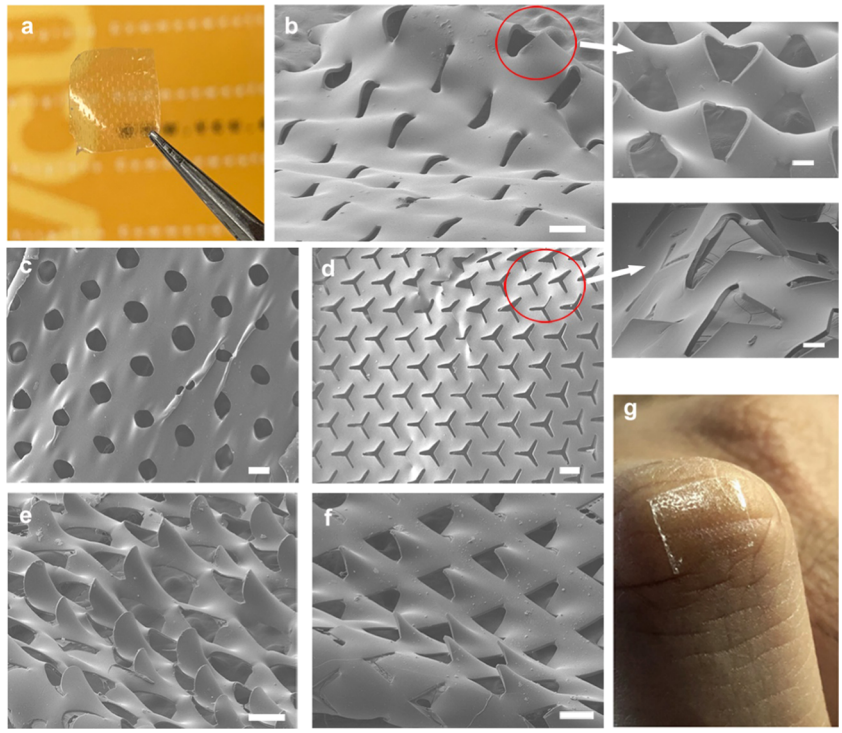

Figure 2. Imaging of silk kirigami (a) large-scale silk kirigami films can be formed that are optically transparent (shown here are cuts 50 μm wide × 500 μm long). SEM images showing the diversity of geometries of cuts that can be formed using photolithography—(b) linear cut geometry with 25 μm cuts, (c) crosscuts that can be stretched biaxially, (d) branched ("*Y*"-cuts), (e) saddles, and (f) chevrons. The top right insets show the out-of-plane deformation of the cuts. (g) Adherence of the film shown in (a) to the skin. The film is moist in this case and remains on during finger flexure. The scale bar on all images = 100 μm. Film thickness = 25 μm.

the traditionally used paper, elastomers (polydimethylsiloxane, PDMS), metal foils, plastics (polyimide, polyethylene terephthalate, polyester films), and graphene-silk composite are among materials reported.[16,17] (Table S1 in the Supporting Information provides several recent examples). To impart conductivity, metal electrodes (Au, Ag, Pt, and Al), indium tin oxide, carbon nanomaterials (nanotubes, graphene), conducting polymers, and 2D layered materials such as MoS_2 have been used.[7,21,24,25] A top-down, lithographic process was shown in a graphene oxide-polyvinyl alcohol nanocomposite with cuts formed using plasma etching through photoresist patterns deposited on the nanocomposite.[22] However, the use of fully biodegradable and biocompatible materials with kirigami strategies has not been shown.

For the first time, photolithographic fabrication of biofunctional, biodegradable silk kirigami via a facile, single-step subtractive process is demonstrated. "Protein lithography" via photoreactive silk fibroin is utilized as a route to multiscale fabrication.[26,27] The biomaterial behaves as a negative-tone photoresist, crosslinking under UV irradiation. Whereas traditional kirigami uses cuts to form desired topologies, a photocurable material permits using photolithography to remove uncrosslinked materials. This results in flexible, free-standing, optically transparent, macroscale sheets with precisely defined microscale cuts. Using finite-element modeling and fracture mechanics, a framework can be established to predict the stretching behavior of these films and their strength, as a function of different cut geometries. Cuts can bring about remarkable "self-shielding" leading to engineered elastic behavior. Silk kirigami sheets are biocompatible, can serve as substrates for cell culture, and be proteolytically degraded. By doping with the conducting

https://dx.doi.org/10.1021/acsami.9b20691
ACS Appl. Mater. Interfaces 2020, 12, 12436−12444

polymer polyaniline (PANI), intrinsically conducting silk kirigami films are demonstrated that are flexible, stretchable, and can be bent and twisted while retaining electrical properties. As mechanically tunable cell scaffolds coupled with electrochemical properties, the use of bioinspired silk kirigami to form degradable and biocompatible, yet functional substrates facilitates advanced capabilities as engineered tissues and (bio)electronic interfaces.[11,28,29]

2. RESULTS AND DISCUSSION

2.1. Fabrication of Flexible Silk Fibroin Kirigami. Kirigami-inspired cuts/patterns using degradable and biocompatible polymers can add a new dimension to their function. Silk proteins form a versatile class of bioresorbable biomaterials for drug delivery, nanostructured scaffolds,[30] and, recently, implantable bioelectronics, photonics, and biointegrated devices.[31,32] Here, microfabrication of flexible, optically transparent kirigami films is realized using a light-reactive silk protein with a rapid, scalable process.[26,33] Material subtraction or cutting is photolithographically accomplished in a single-step process. The solution of photocrosslinkable (silk) fibroin in hexafluoroisopropanol was crosslinked by exposure through a photomask, resulting in complex patterns (Figure 1). As a negative-tone photoresist-like material, an uncrosslinked material is developed, and the resulting free-standing silk kirigami sheet easily peeled off. The sheets formed are stable in a wide range of solvents and can be stored in air or water over several weeks without degradation.[27,33]

The cuts have a high structural fidelity and spatial resolution demonstrating the scalability and accuracy of this photolithographic process to form micropatterns over large areas. Scanning electron microscopy (SEM) imaging shows ordered patterns of various complexities over a large area (cm scale) of flexible fibroin sheets (Figure 2b–f). They are optically transparent (Figure 2a), shown here with cuts −50 μm wide, 500 μm long, enabling potential use in stretchable optics and transparent devices.[34] Cuts down to ∼10 μm using benchtop lithography can be easily formed, with nanoscale patterns possible using electron beam lithography.[35] The microcut kirigami films are mechanically robust and can be held, rolled, or bent into various conformations without any loss in their physicochemical−mechanical properties. Bending certain patterns such as branches, saddles, or chevrons results in interesting and useful microscale openings and out-of-plane deformations (Figures 2 and S1). In an unanticipated result, it was observed that partial cuts, particularly at smaller feature sizes, could be formed by reducing the time of crosslinking. This results in films that can have engineered weakness along with the partial cuts (Figure S2).

Films tens of μm thick are easily formed by controlling the amount of solution cast and the spin-coating speed (films reported here are formed with a thickness of 20−25 μm, confirmed by optical and electron microscopy). While the dry films are flexible but not compliant, moist films can be applied to and readily conform to irregular surfaces (e.g., skin) (Figure 2g) without the need for adhesives. In comparison, a pristine film of a similar size and thickness is quickly delaminated on bending the finger. The results show that moist silk kirigami films display enhanced adhesion to the skin similar to earlier reported laser-cut PDMS.[36] Human skin is known to be stretchable to 75% strain, with surface strains ∼55% at the knees.[37] The introduction of deformability in silk kirigami sheets, with fracture-resistant openings to accommodate stretch, allows highly conformable interfaces or attachment at interfaces.[38]

2.2. Tensile Testing and Finite-Element Modeling. Kirigami-based structural designs can achieve dynamic shaping toward stretchability and foldability.[39] Kirigami sheets possess a mechanical regime in which they are stretchable and soft in comparison to pristine (uncut) sheets.[40] The mechanical properties are dramatically affected by the presence of the cuts resulting in a desired large enhanced deformability but in undesired weakening, as predicted by fracture mechanics. Tensile testing was conducted on thin silk kirigami films with a simple, uniform slit geometry. Experimental values were obtained for two sets of cuts −100 μm wide × 500 μm and 100 μm × 1000 μm long, as well as a branched geometry—*Y*-cuts. Measurements were taken at a strain rate of 0.1 mm/s. Consistent with prior reports, pristine (uncut) silk films have a high breaking stress but fail at strains of ∼7% (Figure S3).[41] In contrast, with a simple cut geometry, even completely dry silk kirigami films can be easily stretched to a strain of ∼40% (Figure 3a—middle panel). The breaking strain recorded is typically below the strain at which the films completely fail. Even though some of the cuts tear, the entire structure does not come apart (Figures S4 and S5). The stills from the tensile test with the point of failure (red-arrow) under load are shown in (Figure S4).

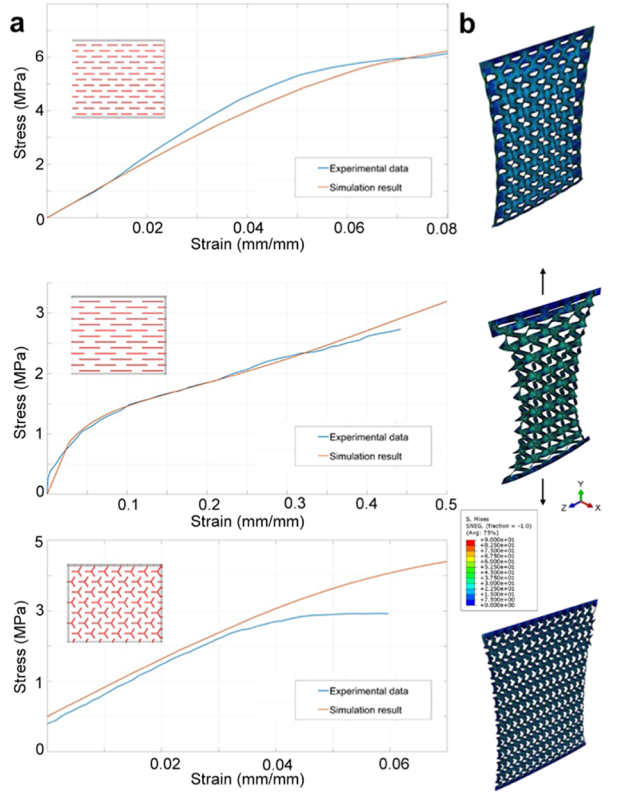

Figure 3. Mechanical behavior experiments and simulations. (a) Stress−strain curves for different kirigami patterns: (top) shorter linear cuts (500 μm), (middle) longer linear cuts (1000 μm), and (bottom) branched cuts (*Y*-shapes) and their respective deformations—(red line: simulation result; blue line: experimental data). The contour plot reports von Mises stress values. (b) Visualization of the finite-element method (FEM) modeling corresponding to the cuts shown. The scale bar shows increasing stress from blue to red.

https://dx.doi.org/10.1021/acsami.9b20691
ACS Appl. Mater. Interfaces 2020, 12, 12436−12444

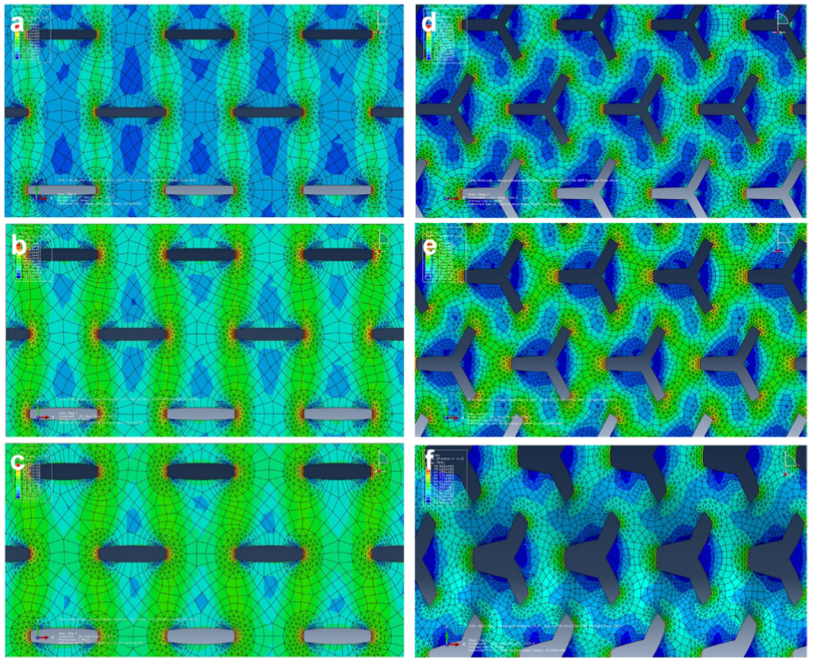

Figure 4. Visualization of the stress concentrations near the cut tips under increasing load conditions (top to bottom 2, 4, and 6 MPa) for a (a–c) slit geometry (500 μm length) and a (d–f) branched (Y-shaped) cut geometry with 200 μm arm length.

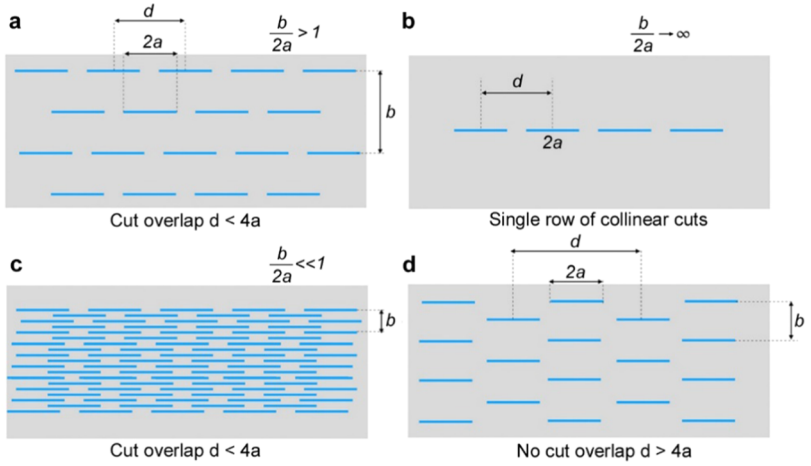

Figure 5. Kirigami patterns as (a, c, d) diamond-shaped array of cuts and (b) single row of collinear cuts.

The stress–strain response was then modeled using the finite-element method (FEM) software ABAQUS, which provides a high level of flexibility, reliability, and verifiability.[19,22,36] A parametric script was used to define different mechanical, geometrical boundary conditions. Input parameters used to perform a specific simulation had varied geometry, material properties (Young's modulus E, Poisson ratio ν, density values of silk fibroin were used), and loading conditions. The mechanical constitutive model is elastoplastic with isotropic linear elasticity and linear hardening. The simulation allows the introduction of a "defect" in correspondence with the middle point of each cut, which triggers the out-of-plane instability typically observed in kirigami structures. This used a preliminary buckling analysis and a nonlinear quasi-static analysis under uniaxial tension. From Figure 3a, the excellent correlation and predictive ability of the simulations with the experimentally observed tensile behavior are noted, even at high strain. The stress visualizations at the crack tips are shown in Figure 4 for the slit geometry and the branched geometry under increasing loads (2–6 MPa). Complete details and videos of the simulations are provided in the Supporting Information. Using the predictive abilities of this FEM analysis, it is possible to ab initio design kirigami geometries for various applications.

2.3. Fracture Mechanics and Design of Self-Shielding Cuts. A mathematical model was developed for the geometries tested to provide a framework for the strength of the silk kirigami films. The model is based on diamond-shaped arrays of "cracks", which are strikingly similar in geometry to the cut patterns.[42,43] Assumptions of linear elastic fracture mechanics, derived from the method of continuous dislocation distributions, were applied. Briefly, considering the geometry shown in Figures 3 and 5, the kirigami shape factor Y depends on the half-length of the cuts (a) and the center-to-center horizontal (d) and vertical separation (b) between two consecutive cuts. Y accounts for the finiteness of the body with respect to the cut

https://dx.doi.org/10.1021/acsami.9b20691
ACS Appl. Mater. Interfaces 2020, 12, 12436–12444

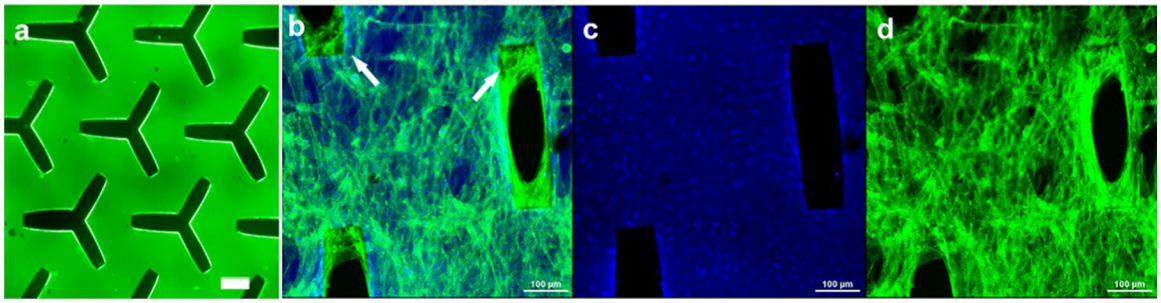

Figure 6. Functionality of silk kirigami (a) Fibroin kirigami films can be loaded with fluorescent dyes (shown here—fluorescein isothiocyanate (FITC)−dextran MW 4 kDa). (b) Adherence of C2C12 cells to the silk kirigami films 7 days after seeding. The arrows show the cytoskeletal bridges across the cuts. (c, d) DAPI and actin staining.

length. For example, a relatively short cut could act as a single central cut in an infinite plane, for which the shape factor is $Y = 1$. If the vertical spacing is large enough ($b/2a \rightarrow \infty$), then the shape factor may be approximated by a single row of collinear cuts (Figure 5b). Its general definition is

$$Y = (1 - s) \tag{1}$$

where $-\infty \leq s \leq 1$ is a calculated self-shielding factor dependent on the cut geometry (Table S2).[43] It is observed that the cut overlaps protect each other resulting in a self-shielding mechanism in the kirigami films. If the vertical spacing is small enough ($b/2a \rightarrow 0$), this shielding mechanism occurs for overlapping rows of cuts (Figure 5a,c). Using these expressions, the critical strength σ_c of the various kirigami geometries and design self-shielding cuts can be estimated.

$$\sigma_c^{\infty} = \frac{K_{I_C}}{Y\sqrt{\pi a}} = \frac{K_{I_C}}{\left(1 - s\left(\frac{b}{2a}, \frac{d}{2a}\right)\right)\sqrt{\pi a}} \tag{2}$$

K_{I_C} is the critical stress intensity factor, estimated using the properties of silk fibroin. Films with longer cuts have a larger cut overlap, resulting in effective shielding. For a cut length of 500 μm, the shape factor is $Y_{500} = 0.65$, while for 1000 μm cuts, the shape factor is $Y_{1000} = 0.3$. The ratio between critical strengths is therefore theoretically estimated to be 1.5, which favorably compares to the experimental value of ∼1.2. A small discrepancy occurs because the technique of continuous dislocation distributions does not account for out-of-plane instability and the plastic hardening observed both experimentally and in FEM simulations. However, these values offer a satisfactory comparison, confirming the design of self-shielding cuts in silk kirigami.

The behavior of patterns with branched cuts can similarly be estimated. The stress intensity factor $K_{I_{br}}$ of a symmetric single branched cut in an infinite medium was estimated using the continuous dislocation distribution technique.[42,44] In this system, the length of the inclined branch (c) = length of the horizontal branch (a) = 200 μm and θ (inclination of the branch) = 60°. It is assumed that the interactions for a diamond-shaped array of straight cuts also apply to a diamond-shaped array of branched cuts. For branched cuts, the vertical separation is b = 866 μm, and horizontal separation is d = 700 μm, corresponding to the condition of cut overlap. The shape factor is $Y_{br} \approx 0.65 = Y_{500}$. Therefore, the ratio of critical strength between the two kirigami with straight and branched cuts is ∼1.7, which only slightly overestimates the strength of the kirigami with branched cuts (ratio ∼ 1.4). Coupled with FEM simulations, such mathematical formulations therefore allow computationally design of self-shielding kirigami cuts with precisely engineered strength and stretchability.

2.4. Evaluation of Biocompatibility and Degradation.

Substrates capable of supporting cell growth and providing topographical and spatial cellular control can deliver insight into the dynamics of cell interactions while providing for ordered cell sheets and cell-based biosensors.[45] Flexible polymeric meshes[46] and ultrathin polymeric films have been previously proposed as functional nanomembranes for directing the cellular organization.[12] Precise micro- and nanoscale surface cuts on a mechanically robust, stretchable biomimetic substrate provide fascinating opportunities to direct the behavior of cells, control cell morphology, interface with tissues, and provide shape programmability.[47] The biocompatibility and noncytotoxicity of the substrate biomaterial were earlier shown.[27] Cell viability was assessed using a 3-(4,5-dimethylthiazol-2-yl)-2,5-diphenyltetrazolium bromide (MTT) assay (Figure S6) showing that the silk kirigami films are conducive to viability and metabolic activity. To verify the potential for cell guidance on silk kirigami, the mouse myoblast cell line C2C12 cells were studied. The kirigami films are robust enough to withstand sterilization procedures allowing for cell patterning (Figure 6). Two different conditions were explored to promote cell attachment—preconditioning with expansion media and coating with human fibronectin. After 7 days of culture, the cell cytoskeleton and nuclei were stained with I-Fluor 488 and 4′,6-diamidino-2-phenylindole (DAPI), respectively, and observed by confocal microscopy. Cells showed adherence to both samples, but a higher and more homogeneous adhesion was observed on kirigami sheets preconditioned with expansion media (Figure 6b−d). This condition had the optimal proliferation rate and organization of the cells. Expectedly, the controls (TCP and uncut fibroin films) also showed good adhesion of cells (Figure S7). DAPI was completely absorbed by the films and used only to show the underlying organization of the cuts (blue films—Figure 6c).

The topographical features of the kirigami design clearly align adhesion along the cuts, guiding the cells via surface morphology. Moreover, the imaging highlights cell alignment on the edges of the cuts and the formation of cytoskeletal bridges linking the sides of the holes (Figure 6b). Similar bridging was observed for fibronectin-coated films (Figure S8). Such flexible, stretchable cell culture sheets can therefore be used for fundamental studies of 3D tissue models, where the cuts can guide cells and the underlying sheets eventually degrade over time. Cuts also provide the opportunity to form

https://dx.doi.org/10.1021/acsami.9b20691
ACS Appl. Mater. Interfaces 2020, 12, 12436−12444

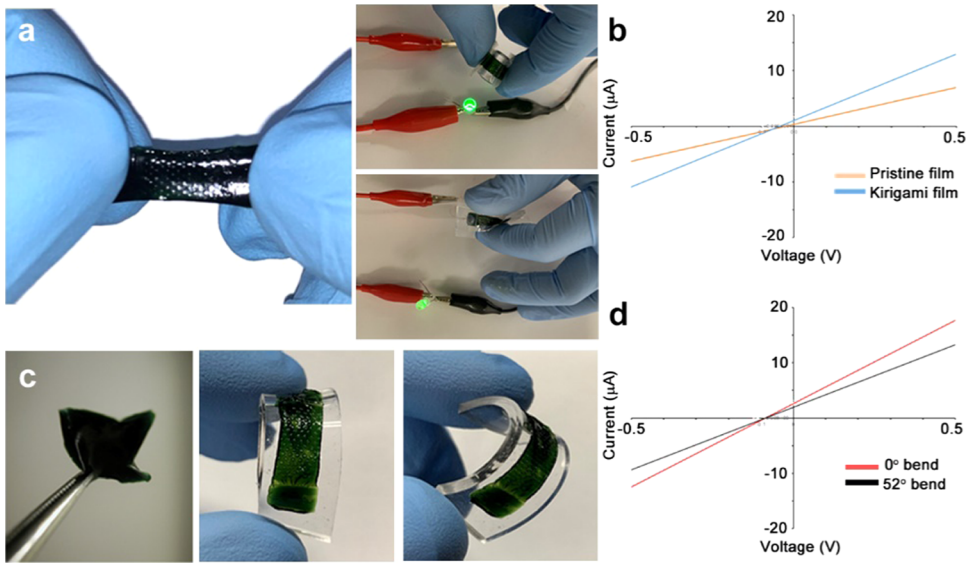

Figure 7. (a) Electrically conducting, mechanically robust kirigami sheets that can be bent and twisted. Films are conductive enough to illuminate a light-emitting diode (LED) under both bending and twisting. (b) Comparison of electrical behavior between a pristine (uncut) film and a kirigami film of a similar size. (c) Sheets can be folded and unfolded. A PDMS slab was used to provide support for measurement under bending. (d) Comparison of behavior in relaxed (0°) and bent (52°) conditions. Film thickness = 25 μm.

sheets with communication and mass transfer between sheets. Biodegradable, free-standing, flexible cell sheets can potentially be stacked to generate 3D multilayered structures, with conformal contact at the biointerface.[48] By dissolving a fluorescent molecule within the fibroin solution, fluorescent kirigami in a variety of designs (Figure 6a) can be formed. In these films, the uniform green fluorescence is derived from FITC−dextran (MW 4 kDa).

An advantage in using silk kirigami in addition to its biocompatibility is the ability of the materials to be controllably degraded in physiological environments. Proteolytic action results in degradation of the silk kirigami sheets leading to the complete loss of mass and structural integrity. An enzymatic biodegradation experiment was conducted on silk kirigami films incubated in the phosphate-buffered saline (PBS) solution with or without protease (control) at 37 °C. Due to proteolytic biodegradation, a loss of weight was observed, and after 10 days, the films incubated in the enzyme broke down, whereas the control samples maintained their integrity and flexibility (Figure S9). This was consistent with previous observations in which the biodegradability of fibroin-based flexible devices can be tuned by controlling the degree of crosslinking and film thickness.[26,33,49] Stretchable devices and biointerfaces with precisely engineered lifetimes can therefore be fabricated using the kirigami films, which can be useful as flexible biomimetic cellular constructs for tissue regeneration, drug delivery platforms, and biosensors.

2.5. Conducting Silk Kirigami. While many soft materials are not potentially degradable or resorbable, conducting polymer composites with silk[50,51] and auxetic patches using chitosan[52] have been used toward tissue-interfacing electronics and e-textiles.[10,39,53] The graphene oxide biopaper was reported with high electrical conductivity.[54] It may be noted that this was primarily graphene oxide, with only 2−5% of silk fibroin to provide binding interactions. Silk-based bioelectronics has the potential for advanced bioapplications, primarily as a bioresorbable substrate for ultrathin electronics.[31] Multifunctional kirigami with intrinsic electrical conductivity is demonstrated by incorporating the conducting polymer polyaniline (PANI) to form fully organic electroactive sheets. PANI has high-temperature resistance, environmental stability, and excellent electrical conductivity.[55] While PANI solubility is typically low in most solvents, it is dispersible in the benign solvent formic acid, which makes it suitable to form silk composites.[33] Initially, compositions were optimized for both electrochemical and mechanical properties. The presence of H-bonding between the benzene ring structures of the molecular backbone of PANI causes rigidity in the composite films making the films brittle at high concentrations.[55] High PANI concentrations impart a dark color to the films, making photolithography difficult (e.g., cuts <100 μm are not easily formed). Poly(ethylene glycol) (PEG, 1%) as a plasticizer was used to improve the flexibility of the silk sheets at optimal PANI concentrations (11% w/w), resulting in mechanically robust and flexible films (Figure 7a).

Conducting kirigami films were made in a similar manner, via UV crosslinking through a photomask followed by development. The electrical conductivity was probed by forming connecting pads at the ends (Figure S10). Initially, kirigami films were compared to pristine (uncut) films of a similar size. For the sake of simplicity, the linear cut geometry was tested. The difference in conductivity (Figure 7b) indicates that the properties of the films are a function of the cut geometry. Excellent conductive behavior was observed (μS conductance levels and linear behavior over a voltage range of −0.5 − +0.5 V). The films (slit width 100 μm, length 500 μm, gap spacing −500 μm, and gap width 500 μm, 25 μm thick) retain their conductivity under stretch (Figure S11), although the conductance changes ∼40% under 10% linear strain. An underlying PDMS slab was used as a support to precisely control the angle of the bend and the twist (Figures 7c and S12). A bend of 50−55° was performed in these experiments to simulate the bending at the knee.[37] The films themselves are stable and function independently of the support. A change in conductance from 3.03 to 2.35 μS (∼22%) was observed in the film on 55° bend. The

https://dx.doi.org/10.1021/acsami.9b20691
ACS Appl. Mater. Interfaces 2020, 12, 12436−12444

conductance changes as a function of stretch and also bending, which indicates that the composites undergo conformational changes on mechanical deformation. However, the films remain conductive under twist and 180° bend (Figure 7d). Coupled with the deformability and stretchability shown, these intrinsically conducting silk kirigami films can therefore be designed for skin-like devices, with a better understanding of the electrochemical behavior linked to the dynamics of deformation.[38] As bioinspired and degradable platforms can be formed in a green fashion, this platform can go a long way toward addressing sustainability in bioelectronics.[56]

3. CONCLUSIONS

In summary, the fabrication of multifunctional silk kirigami films using a facile photolithographic technique is demonstrated. The kirigami films themselves are simultaneously extremely stretchable and robust thanks to self-shielding cuts and can be formed at various thicknesses ranging from thin (ca. μm) to thick (10 s of microns), as well as degradable. The cut geometries of these films can be easily engineered via light-assisted microfabrication, which permits the formation of complex, high-resolution architectures at high throughput and scale. The computational FEM and theoretical fracture mechanics models guide and support the experimental findings and provide insight into the modes of deformation and fracture including the presence of self-shielding cuts and the influence of geometry. Critically, these silk kirigami films are biocompatible and display the ability to spatially direct cell growth along the cut geometry, while also being controllably biodegradable. It is also possible to modulate the electrochemical characteristics of the films by doping with the conducting polymer polyaniline. These results suggest that silk kirigami can provide exceptional bioinspired and biodegradable structures toward flexible and stretchable biodevices.

4. EXPERIMENTAL SECTION

4.1. Fabrication of Micropatterned Kirigami Films Using Photocrosslinkable Fibroin. Photocrosslinkable fibroin (referred to as fibroin protein photoresist or photofibroin) was prepared by the incorporation of photoreactive moieties to fibroin as reported earlier.[26] The photofibroin (7.5% (w/v)) was dissolved in hexafluoroisopropanol (HFIP) with the 2.5% (w/v) photoinitiator (Irgacure 2959, BASF). The solution was drop cast on plain glass slides and air-dried for 15 min to evaporate the excess solvent. Samples were crosslinked using 365 nm UV (Lumen Dynamics OmniCure 1000) at 20 mW/cm^2. Uncrosslinked areas (cuts) were developed by soaking in 1 M LiCl/dimethyl sulfoxide (DMSO). Free-standing films were obtained by soaking developed films in deionized water to delaminate them from the glass support. Films were washed in water and stored in air or water. To form conducting fibroin films, polyaniline (PANI) emeraldine salt from *p*-toluenesulfonic acid (Alfa Aesar, Tewksbury, MA) (11% w/w) and photofibroin were dissolved in formic acid. Similar fabrication steps were followed.

4.2. Electrochemical Characterization. Linear sweep voltammetry (LSV) was used to characterize the electrochemical properties of the silk-PANI kirigami films. The measurement was conducted by a Gamry Interface 1010E Potentiostat (Gamry Instruments, Warminster, PA). The scanning range of applied potential was from −0.5 to 0.5 V (over 1 V) with a rate of 100 mV/s. The electrochemical data was analyzed using the Gamry Echem Analyst software. Electrical connections were tested by connecting to a DC power source.

4.3. Tensile Tests. Kirigami samples were fixed on a paper frame with a window of 0.5 cm side. The tensile test was performed on an MTS 300 series tensile testing machine (MTS Systems Corporation, Eden Prairie, MN) equipped with a 50 N load cell. Measurements were taken at a strain rate of 0.1 mm/s, and data was collected at a rate of 10 Hz. All other parameters are sample-specific such as thickness, width, and length. Typically, films were 20−25 μm thick.

4.4. Finite-Element Modeling and Simulation. The commercial software ABAQUS was used to compute the deformations of the kirigami films for the three patterns in Figure 3a. The mesh is composed of 6-node triangular thin shell elements (STRI65) near the tips to limit element distortion upon cut opening and 8-node quadrangular thin shells (S8R5) for the rest of the domain. A convergence analysis through mesh refinement was conducted to ensure mathematical accuracy. The final ratio between average mesh size (and the width of the films was 560) and the cut width was 4. An elastoplastic isotropic linear elastic constitutive model, with linear hardening was used. The material properties are Young's Modulus 248 MPa, Poisson's ratio 0.3, yield stress 12.92 MPa, and hardening coefficient 26.36 MPa. To stabilize the dynamic implicit simulations, artificial numerical damping is introduced (by setting the parameters $\alpha = -0.41421$, $\beta = 0.5$, and $\gamma = 0.91421$ in the Hilber−Hughes−Taylor time integration). Quasi-static conditions are ensured by monitoring the kinetic energy.

4.5. Cell Culture Experiments. Mouse muscle myoblast cells (C2C12) were expanded in medium consisting in Dulbecco's modified Eagle medium (DMEM) high glucose (Euroclone), 10% fetal bovine serum (Euroclone), 1% antibiotic/antimycotic (Euroclone), 1% L-glutamine (Euroclone), and 1% sodium pyruvate (GIBCO). Cells were cultured in a 75 cm^2 flask at 37 °C and 5% CO_2 in a humidified atmosphere and expanded until 70% confluence was reached. For this experiment, the cell passage was 16. Samples were pretreated by two different methods—one group was preconditioned with the complete expansion medium at 37 °C for 30 min, the other was incubated with human fibronectin (Sigma-Aldrich) for 1 h at 37 °C. As a control, silk fibroin sheets without cuts were used and preconditioned with a complete expansion medium and with human fibronectin, as kirigami films. All samples were sterilized with 70% ethanol for 40 min and then washed twice with sterile PBS (Euroclone).

4.6. Morphological Evaluation of Adhered Cells. Adhered cell morphology on kirigami sheets was studied by imagining by confocal microscopy on day 7 after seeding using a Nikon A1 laser microscope. Before confocal observations, samples were fixed with 4% PFA for 40 min, permeabilized with 0.2% Triton X-100 for 30 min. The nuclei and the cell cytoskeleton were stained with DAPI (Sigma-Aldrich) and I-Fluor 488 (Abcam), respectively, per the manufacturers' instruction.

4.7. Proteolytic Degradation in Vitro. Silk fibroin films can be proteolytically degraded over time in the presence of enzymes. In the present work, the degradation of silk kirigami films in the presence of protease (Protease XIV from *Streptomyces griseus*, ≥3.5 U/mg, Sigma-Aldrich) was demonstrated. Films, 20 μm thick with 100 μm cuts (containing ∼2.5 mg fibroin), were incubated in 5 mL of protease (1 U/mg of protein) at 37 °C, and the degradation was studied over 2 weeks. Note that this protease concentration is ∼3× the prior used concentrations, resulting in a comparatively rapid degradation.[26,33,49] Another set of samples was incubated in PBS buffer under the same environment, which served as the negative control. The enzyme solution was replaced every 3 days to maintain protease activity. Samples from each set were taken out on different days, rinsed with deionized (DI) water, and imaged under a microscope to record their degradation over time.

■ ASSOCIATED CONTENT

Supporting Information

The Supporting Information is available free of charge at https://pubs.acs.org/doi/10.1021/acsami.9b20691.

Kirigami literature, additional images of the silk kirigami, MTT assay, cellular spreading, mathematical modeling, simulations, tensile behavior, and conductive silk kirigami are provided; examples of different materials and fabrication techniques used to form kirigami cuts

https://dx.doi.org/10.1021/acsami.9b20691
ACS Appl. Mater. Interfaces 2020, 12, 12436−12444

(Table S1); scanning electron microscopy (SEM) images of large-area microscale silk kirigami films with different pattern geometries (Figure S1); reducing the exposure time (in this experiment, the exposure time was 1 s), it is possible to engineer weak spots in the films in the form of unopened or partial cuts (Figure S2) (PDF)

Stress−strain curves for different kirigami patterns: (top) shorter linear cuts (500 μm), (middle) longer linear cuts (1000 μm), and (bottom) branched cuts (*Y*-shapes) and their respective deformations (AVI)

Visualization of the FEM modeling corresponding to the cuts shown; scale bar shows increasing stress from blue to red (AVI)

AUTHOR INFORMATION

Corresponding Authors

Nicola M. Pugno − *Laboratory of Bio-inspired, Bionic, Nano, Meta Materials & Mechanics, Department of Civil, Environmental and Mechanical Engineering, University of Trento, 38122 Trento, Italy; Fondazione Edoardo Amaldi, 00133 Rome, Italy; School of Engineering and Materials Science, Queen Mary University of London, London E1 4NS, United Kingdom;* orcid.org/0000-0003-2136-2396; Email: nicola.pugno@unitn.it

Vamsi K. Yadavalli − *Department of Chemical and Life Science Engineering, Virginia Commonwealth University, Richmond, Virginia 23284, United States;* orcid.org/0000-0002-8879-1948; Email: vyadavalli@vcu.edu

Authors

Sayantan Pradhan − *Department of Chemical and Life Science Engineering, Virginia Commonwealth University, Richmond, Virginia 23284, United States*

Leonardo Ventura − *School of Engineering and Materials Science, Queen Mary University of London, London E1 4NS, United Kingdom*

Francesca Agostinacchio − *BIOtech Research Center, Department of Industrial Engineering, University of Trento, 38122 Trento, Italy*

Meng Xu − *Department of Chemical and Life Science Engineering, Virginia Commonwealth University, Richmond, Virginia 23284, United States*

Ettore Barbieri − *Japan Agency for Marine-Earth Science and Technology, Center for Mathematical Science and Advanced Technology, Computational Science and Engineering Group, Yokohama, Kanagawa 236-0001, Japan*

Antonella Motta − *BIOtech Research Center, Department of Industrial Engineering, University of Trento, 38122 Trento, Italy*

Complete contact information is available at: https://pubs.acs.org/10.1021/acsami.9b20691

Notes

The authors declare no competing financial interest.

ACKNOWLEDGMENTS

This research was partly supported by funding from the National Science Foundation (CBET-1704435). SEM images were obtained at the VCU Nanomaterials Characterization Center. NMP is supported by the European Commission under the Graphene Flagship Core 2 grant No. 785219 (WP14 "Composites") and FET Proactive "Neurofibres" grant No. 732344, the FET Open (Boheme) grant No. 863179, as well as by the Italian Ministry of Education, University and Research (MIUR), under the "Departments of Excellence" grant L. 232/2016, the ARS01-01384-PROSCAN Grant, and the PRIN-20177TTP3S. EB is supported by JSPS KAKENHI Grant Number JP18K18065 and the Cross-Ministerial Strategic Innovation Promotion (SIP) Program for Deep Ocean Resources.

REFERENCES

(1) Jeong, J. W.; Yeo, W. H.; Akhtar, A.; Norton, J. J.; Kwack, Y. J.; Li, S.; Jung, S. Y.; Su, Y.; Lee, W.; Xia, J. Materials and Optimized Designs for Human-Machine Interfaces via Epidermal Electronics. *Adv. Mater.* **2013**, *25*, 6839−6846.

(2) Cai, P.; Hu, B.; Leow, W. R.; Wang, X.; Loh, X. J.; Wu, Y. L.; Chen, X. Biomechano-Interactive Materials and Interfaces. *Adv. Mater.* **2018**, *30*, No. 1800572.

(3) Lendlein, A.; Trask, R. S. Multifunctional Materials: Concepts, Function-Structure Relationships, Knowledge-Based Design, Translational Materials Research. *Multifunct. Mater.* **2018**, *1*, No. 010201.

(4) Lu, N. S.; Kim, D. H. Flexible and Stretchable Electronics Paving the Way for Soft Robotics. *Soft Robotics* **2014**, *1*, 53−62.

(5) Hammock, M. L.; Chortos, A.; Tee, B. C. K.; Tok, J. B. H.; Bao, Z. 25th anniversary article: The Evolution of Electronic Skin (E-Skin): A Brief History, Design Considerations, and Recent Progress. *Adv. Mater.* **2013**, *25*, 5997−6038.

(6) Kim, D. H.; Lu, N. S.; Ma, R.; Kim, Y. S.; Kim, R. H.; Wang, S. D.; Wu, J.; Won, S. M.; Tao, H.; Islam, A.; Yu, K. J.; Kim, T. I.; Chowdhury, R.; Ying, M.; Xu, L. Z.; Li, M.; Chung, H. J.; Keum, H.; McCormick, M.; Liu, P.; Zhang, Y. W.; Omenetto, F. G.; Huang, Y. G.; Coleman, T.; Rogers, J. A. Epidermal Electronics. *Science* **2011**, *333*, 838−843.

(7) Matsuhisa, N.; Chen, X.; Bao, Z.; Someya, T. Materials and Structural Designs of Stretchable Conductors. *Chem. Soc. Rev.* **2019**, *48*, 2946−2966.

(8) Xu, S.; Yan, Z.; Jang, K.-I.; Huang, W.; Fu, H.; Kim, J.; Wei, Z.; Flavin, M.; McCracken, J.; Wang, R. Assembly of Micro/nanomaterials into Complex, Three-dimensional Architectures by Compressive Buckling. *Science* **2015**, *347*, 154−159.

(9) Lu, T.; Finkenauer, L.; Wissman, J.; Majidi, C. Rapid prototyping for Soft-matter Electronics. *Adv. Funct. Mater.* **2014**, *24*, 3351−3356.

(10) Chortos, A.; Liu, J.; Bao, Z. Pursuing Prosthetic Electronic Skin. *Nat. Mater.* **2016**, *15*, 937−950.

(11) Feiner, R.; Dvir, T. Tissue−electronics interfaces: From Implantable Devices to Engineered Tissues. *Nat. Rev. Mater.* **2018**, *3*, No. 17076.

(12) Fujie, T. Development of Free-standing Polymer Nanosheets for Advanced Medical and Health-care Applications. *Polym. J.* **2016**, *48*, 773−780.

(13) Li, J.; Li, G.; Zhang, K.; Liao, Y.; Yang, P.; Maitz, M. F.; Huang, N. Co-Culture of Vascular Endothelial Cells and Smooth Muscle Cells by Hyaluronic Acid Micro-Pattern on Titanium Surface. *Appl. Surf. Sci.* **2013**, *273*, 24−31.

(14) Meco, E.; Lampe, K. J. Microscale Architecture in Biomaterial Scaffolds for Spatial Control of Neural Cell Behavior. *Front. Mater.* **2018**, *5*, No. 1593.

(15) Lantigua, D.; Kelly, Y. N.; Unal, B.; Camci-Unal, G. Engineered Paper-based Cell Culture Platforms. *Adv. Healthcare Mater.* **2017**, *6*, No. 1700619.

(16) Ning, X.; Wang, X.; Zhang, Y.; Yu, X.; Choi, D.; Zheng, N.; Kim, D. S.; Huang, Y.; Zhang, Y.; Rogers, J. A. Assembly of Advanced Materials into 3D Functional Structures by Methods Inspired by Origami and Kirigami: A Review. *Adv. Mater. Interfaces* **2018**, *5*, No. 1800284.

(17) Xu, L.; Shyu, T. C.; Kotov, N. A. Origami and Kirigami Nanocomposites. *ACS Nano* **2017**, *11*, 7587−7599.

(18) Chen, B. G.; Liu, B.; Evans, A. A.; Paulose, J.; Cohen, I.; Vitelli, V.; Santangelo, C. Topological Mechanics of Origami and Kirigami. *Phys. Rev. Lett.* **2016**, *116*, No. 135501.
(19) Vachicouras, N.; Tringides, C. M.; Campiche, P. B.; Lacour, S. P. Engineering Reversible Elasticity in Ductile and Brittle Thin Films Supported by a Plastic Foil. *Extreme Mech. Lett.* **2017**, *15*, 63−69.
(20) Groeger, D.; Steimle, J. In *LASEC: Instant Fabrication of Stretchable Circuits Using a Laser Cutter*, Proceedings of the 2019 CHI Conference on Human Factors in Computing Systems, Glasgow, U.K., 2019; pp 1−14.
(21) Blees, M. K.; Barnard, A. W.; Rose, P. A.; Roberts, S. P.; McGill, K. L.; Huang, P. Y.; Ruyack, A. R.; Kevek, J. W.; Kobrin, B.; Muller, D. A. Graphene kirigami. *Nature* **2015**, *524*, 204−207.
(22) Shyu, T. C.; Damasceno, P. F.; Dodd, P. M.; Lamoureux, A.; Xu, L.; Shlian, M.; Shtein, M.; Glotzer, S. C.; Kotov, N. A. A Kirigami Approach to Engineering Elasticity in Nanocomposites through Patterned Defects. *Nat. Mater.* **2015**, *14*, 785−789.
(23) Lamoureux, A.; Lee, K.; Shlian, M.; Forrest, S. R.; Shtein, M. Dynamic Kirigami Structures for Integrated Solar Tracking. *Nat. Commun.* **2015**, *6*, No. 8092.
(24) Zheng, W.; Huang, W.; Gao, F.; Yang, H.; Dai, M.; Liu, G.; Yang, B.; Zhang, J.; Fu, Y. Q.; Chen, X. Kirigami-Inspired Highly Stretchable Nanoscale Devices Using Multidimensional Deformation of Monolayer MoS2. *Chem. Mater.* **2018**, *30*, 6063−6070.
(25) Hu, K.; Gupta, M. K.; Kulkarni, D. D.; Tsukruk, V. V. Ultra-robust Graphene Oxide-silk Fibroin Nanocomposite Membranes. *Adv. Mater.* **2013**, *25*, 2301−2307.
(26) Kurland, N. E.; Dey, T.; Kundu, S. C.; Yadavalli, V. K. Precise Patterning of Silk Microstructures Using Photolithography. *Adv. Mater.* **2013**, *25*, 6207−6212.
(27) Xu, M.; Pradhan, S.; Agostinacchio, F.; Pal, R. K.; Greco, G.; Mazzolai, B.; Pugno, N. M.; Motta, A.; Yadavalli, V. K. Easy, Scalable, Robust, Micropatterned Silk Fibroin Cell Substrates. *Adv. Mater. Interfaces* **2019**, *6*, No. 1801822.
(28) Muskovich, M.; Bettinger, C. J. Biomaterials-Based Electronics: Polymers and Interfaces for Biology and Medicine. *Adv. Healthcare Mater.* **2012**, *1*, 248−266.
(29) Irimia-Vladu, M. "Green" electronics: Biodegradable and Biocompatible Materials and Devices for Sustainable Future. *Chem. Soc. Rev.* **2014**, *43*, 588−610.
(30) Omenetto, F. G.; Kaplan, D. L. New Opportunities for an Ancient Material. *Science* **2010**, *329*, 528−531.
(31) Hwang, S. W.; Kim, D. H.; Tao, H.; Kim, T. I.; Kim, S.; Yu, K. J.; Panilaitis, B.; Jeong, J. W.; Song, J. K.; Omenetto, F. G.; Rogers, J. A. Materials and Fabrication Processes for Transient and Bioresorbable High-Performance Electronics. *Adv. Funct. Mater.* **2013**, *23*, 4087−4093.
(32) Tao, H.; Kainerstorfer, J. M.; Siebert, S. M.; Pritchard, E. M.; Sassaroli, A.; Panilaitis, B. J. B.; Brenckle, M. A.; Amsden, J. J.; Levitt, J.; Fantini, S.; Kaplan, D. L.; Omenetto, F. G. Implantable, Multifunctional, Bioresorbable Optics. *Proc. Natl. Acad. Sci. U.S.A.* **2012**, *109*, 19584−19589.
(33) Bucciarelli, A.; Pal, R. K.; Maniglio, D.; Quaranta, A.; Mulloni, V.; Motta, A.; Yadavalli, V. K. Fabrication of Nanoscale Patternable Films of Silk Fibroin Using Benign Solvents. *Macromol. Mater. Eng.* **2017**, *302*, No. 1700110.
(34) Kim, K.; Park, Y. G.; Hyun, B. G.; Choi, M.; Park, J. U. Recent Advances in Transparent Electronics with Stretchable Forms. *Adv. Mater.* **2019**, *31*, No. 1804690.
(35) Pal, R. K.; Yadavalli, V. K. Silk Protein Nanowires Patterned using Electron Beam Lithography. *Nanotechnology* **2018**, *29*, No. 335301.
(36) Zhao, R.; Lin, S.; Yuk, H.; Zhao, X. Kirigami Enhances Film Adhesion. *Soft Matter* **2018**, *14*, 2515−2525.
(37) Yamada, T.; Hayamizu, Y.; Yamamoto, Y.; Yomogida, Y.; Izadi-Najafabadi, A.; Futaba, D. N.; Hata, K. A Stretchable Carbon Nanotube Strain Sensor for Human-motion Detection. *Nat. Nanotechnol.* **2011**, *6*, 296−301.
(38) Wang, S.; Oh, J. Y.; Xu, J.; Tran, H.; Bao, Z. Skin-inspired Electronics: an Emerging Paradigm. *Acc. Chem. Res.* **2018**, *51*, 1033−1045.
(39) Wang, C.; Wang, C.; Huang, Z.; Xu, S. Materials and Structures toward Soft Electronics. *Adv. Mater.* **2018**, *30*, No. 1801368.
(40) Isobe, M.; Okumura, K. Initial Rigid Response and Softening Transition of Highly Stretchable Kirigami Sheet Materials. *Sci. Rep.* **2016**, *6*, No. 24758.
(41) Jiang, C.; Wang, X.; Gunawidjaja, R.; Lin, Y. H.; Gupta, M. K.; Kaplan, D. L.; Naik, R. R.; Tsukruk, V. V. Mechanical Properties of Robust Ultrathin Silk Fibroin Films. *Adv. Funct. Mater.* **2007**, *17*, 2229−2237.
(42) Bilby, B. A.; Cottrell, A. H.; Swinden, K. The Spread of Plastic Yield from a Notch. *Proc. R. Soc. A* **1963**, *272*, 304−314.
(43) Delameter, W.; Herrmann, G. Weakening of Elastic Solids by Doubly-periodic Arrays of Cracks. In *Topics in Applied Continuum Mechanics*; Springer, 1974; pp 156−173.
(44) Chen, Y.; Hasebe, N. New Integration Scheme for the Branch Crack Problem. *Eng. Fract. Mech.* **1995**, *52*, 791−801.
(45) Feinberg, A. W.; Feigel, A.; Shevkoplyas, S. S.; Sheehy, S.; Whitesides, G. M.; Parker, K. K. Muscular Thin Films for Building Actuators and Powering Devices. *Science* **2007**, *317*, 1366−1370.
(46) Gong, M.; Wan, P.; Ma, D.; Zhong, M.; Liao, M.; Ye, J.; Shi, R.; Zhang, L. Flexible Breathable Nanomesh Electronic Devices for On-Demand Therapy. *Adv. Funct. Mater.* **2019**, *29*, No. 1902127.
(47) Studart, A. R.; Erb, R. M. Bioinspired Materials that Self-shape through Programmed Microstructures. *Soft Matter* **2014**, *10*, 1284−1294.
(48) Haraguchi, Y.; Shimizu, T.; Sasagawa, T.; Sekine, H.; Sakaguchi, K.; Kikuchi, T.; Sekine, W.; Sekiya, S.; Yamato, M.; Umezu, M. Fabrication of Functional Three-dimensional Tissues by Stacking Cell Sheets in vitro. *Nat. Protoc.* **2012**, *7*, 850−858.
(49) Pal, R. K.; Farghaly, A. A.; Wang, C.; Collinson, M. M.; Kundu, S. C.; Yadavalli, V. K. Conducting Polymer-silk Biocomposites for Flexible and Biodegradable Electrochemical Sensors. *Biosens. Bioelectron.* **2016**, *81*, 294−302.
(50) Lund, A.; Darabi, S.; Hultmark, S.; Ryan, J. D.; Andersson, B.; Ström, A.; Müller, C. Roll-to-Roll Dyed Conducting Silk Yarns: A Versatile Material for E-Textile Devices. *Adv. Mater. Technol.* **2018**, *3*, No. 1800251.
(51) Müller, C.; Hamedi, M.; Karlsson, R.; Jansson, R.; Marcilla, R.; Hedhammar, M.; Inganäs, O. Woven Electrochemical Transistors on Silk Fibers. *Adv. Mater.* **2011**, *23*, 898−901.
(52) Kapnisi, M.; Mansfield, C.; Marijon, C.; Guex, A. G.; Perbellini, F.; Bardi, I.; Humphrey, E. J.; Puetzer, J. L.; Mawad, D.; Koutsogeorgis, D. C. Auxetic Cardiac Patches with Tunable Mechanical and Conductive Properties toward Treating Myocardial Infarction. *Adv. Funct. Mater.* **2018**, *28*, No. 1800618.
(53) Lipomi, D. J.; Bao, Z. Stretchable and Ultraflexible Organic Electronics. *MRS Bull.* **2017**, *42*, 93−97.
(54) Hu, K.; Xiong, R.; Guo, H.; Ma, R.; Zhang, S.; Wang, Z. L.; Tsukruk, V. V. Self-Powered Electronic Skin with Biotactile Selectivity. *Adv. Mater.* **2016**, *28*, 3549−3556.
(55) Sen, T.; Mishra, S.; Shimpi, N. G. Synthesis and Sensing Applications of Polyaniline Nanocomposites: A Review. *RSC Adv.* **2016**, *6*, 42196−42222.
(56) Torculas, M.; Medina, J.; Xue, W.; Hu, X. Protein-based Bioelectronics. *ACS Biomater. Sci. Eng.* **2016**, *2*, 1211−1223.

https://dx.doi.org/10.1021/acsami.9b20691
ACS Appl. Mater. Interfaces 2020, 12, 12436−12444

Supporting information for manuscript

Biofunctional silk kirigami with engineered properties

Sayantan Pradhan, Leonardo Ventura, Francesca Agostinacchio, Meng Xu, Ettore Barbieri, Antonella Motta, Nicola M. Pugno, Vamsi K Yadavalli *

S. Pradhan, Dr. M. Xu, Dr. V. K. Yadavalli
Department of Chemical and Life Science Engineering
Virginia Commonwealth University
601 W Main Street, Richmond VA, USA 23284
E-mail: vyadavalli@vcu.edu

F. Agostinacchio, Prof. A. Motta
BIOtech Research Center
Department of Industrial Engineering
University of Trento, TN, Italy

Dr. E. Barbieri
Japan Agency for Marine-Earth Science and Technology
Center for Mathematical Science and Advanced Technology
Computational Science and Engineering Group
3173-25, Showa-machi, Kanazawa-ku, Yokohama-city, Kanagawa, 236-0001, Japan

Prof. N. M. Pugno
Laboratory of Bio-Inspired & Graphene Nanomechanics,
Department of Civil, Environmental and Mechanical Engineering,
University of Trento, TN, Italy
&
Fondazione Edoardo Amaldi, Via del Politecnico snc, Rome, Italy

L. Ventura, Prof. N. M. Pugno
School of Engineering and Materials Science,
Queen Mary University of London, L, United Kingdom

Keywords: silk fibroin, flexible kirigami, micropatterning, conducting polymer, biodegradable

Table S1 – Examples of different materials and fabrication techniques used to form kirigami cuts.

Materials	**Fabrication method**	**Dimensions/shape**	**Applications**	**Ref.**
poly(3-butylthiophene-2,5-diyl) (P3BT) in poly[(9,9-dioctylfluorenyl-2,7-diyl)-*co*-(4,4′-(*N*-(4-*sec*-butylphenyl)diphenylamine)] (TFB) matrix	Laser cutting	Staggered linear cuts Length of cuts x the gap of horizontal cuts x the space of vertical staggered cuts (16x3.2x0.5, 36x2.8x0.6, 48x3.5x0.9, 62x4.2x0.6 mm)	A highly stretchable, foldable, and twistable conductor for light-emitting diode (LED).	[1]
PET films coated with conductive materials (ITO, Ag, PEDOT: PSS, carbon)	Laser cutting	Staggered linear and Y-shape cuts (15 mm and 5 mm)	Interactive transparent wristband, 3D-printed stretchable game controller, textile sensor patch for joint angle estimation	[2]
Graphene oxide/PVA	Photolithography, followed by oxygen plasma etching	Staggered linear cuts (500 μm)	---	[3]
Graphite electrodes on polyimide sheet	CO_2 laser	Staggered linear cuts (over 3 cm)	Stretchable supercapacitor	[4]
Gold nanofilms	Dual-beam focused ion beam (FIB)/SEM system	Arcs and 3D microdome (sub-50-nm)	3D optical chirality	[5]
Polycrystalline monolayer graphene grown on copper	Optical lithography	In plane kirigami springs, out of plane pyramidal spring	Conductivity of the springs and environment responsive actuation of out of plane kirigami structure	[6]
Thin film gallium arsenide	Photolithography and chemical etching	Staggered linear cuts	Thin-film GaAs solar cells and a kirigami tracker made from Kapton sheet	[7]
PET and PDMS films with PEDOT:PSS and CNT	Laser cutting	Staggered lines	Wearable health monitoring device with temperature, ECG, UV and a 3 axis acceleration sensor	[8]
Gold traces embedded in Parylene C	Oxygen plasma etching	Serpentine cuts	Flexible strain sensor	[9]
Mono-layer molybdenum disulfide on PDMS	Molding and plasma etching	Linear patterns of kirigami springs, kirigami pyramids, and out-of-plane kirigami springs with alternating C-shapes	Strain sensor	[10]
Graphene oxide- silk fibroin biocomposite	Drag knife cutting	Staggered lines, pop-up box, spiral slinky, spinner, parallel lines	Energy harvester/ triboelectric nanogenerator	[11]
$LiFePO_4$ (LFP) or $Li_4Ti_5O_{12}$ (LTO),	Template printing	Staggered lines	Stretchable battery	[12]

poly(vinylidene fluoride) (PVDF), and multiwalled carbon nanotubes (MWCNTs; conductive additive) mixed in N-methyl-2-pyrrolidone (NMP)				
Paper and pre-strained shape memory polymer-based shrink paper	Laser cutting	Square and triangle cuts	Programmable 3D self-folding kirigami machines and soft turning robots	[13]
Super-stretchable abrasion resistant natural rubber, PDMS	Laser cutting, molding	Perpendicular lines	Shape-morphing mechanical metamaterials	[14]

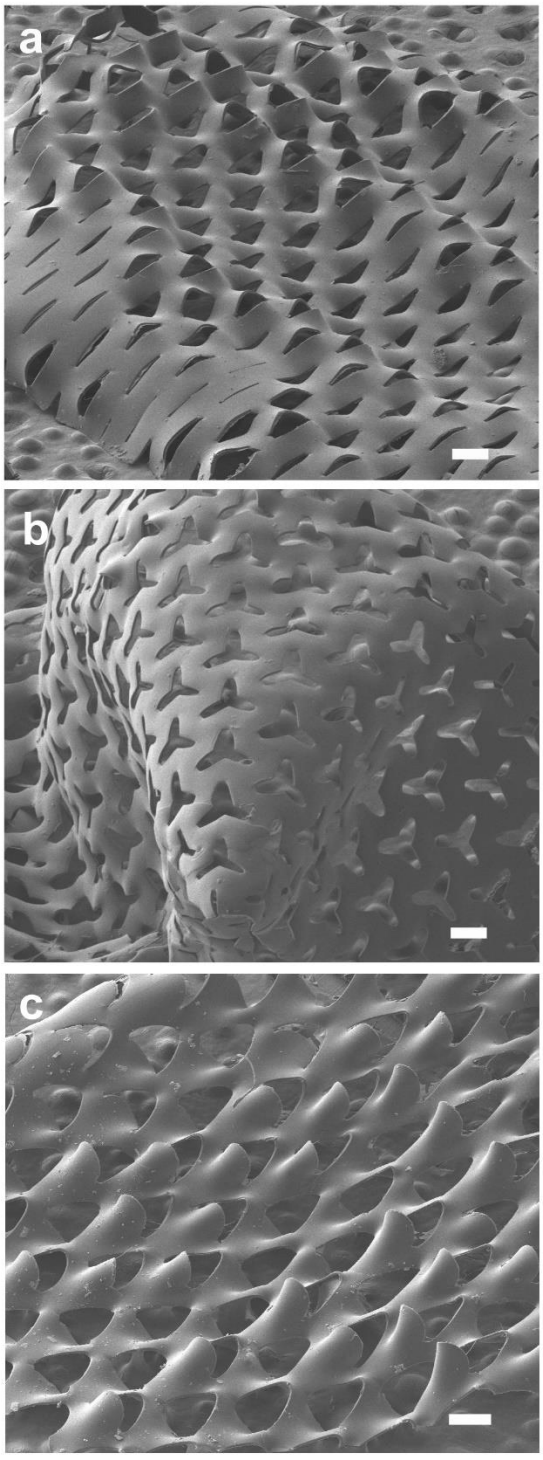
a
b
c

Figure S1 – Scanning Electron Microscopy (SEM) images of large area microscale silk kirigami films with different pattern geometries (top to bottom – (a) slits, (b) Y-cuts, and (c) saddle shapes).

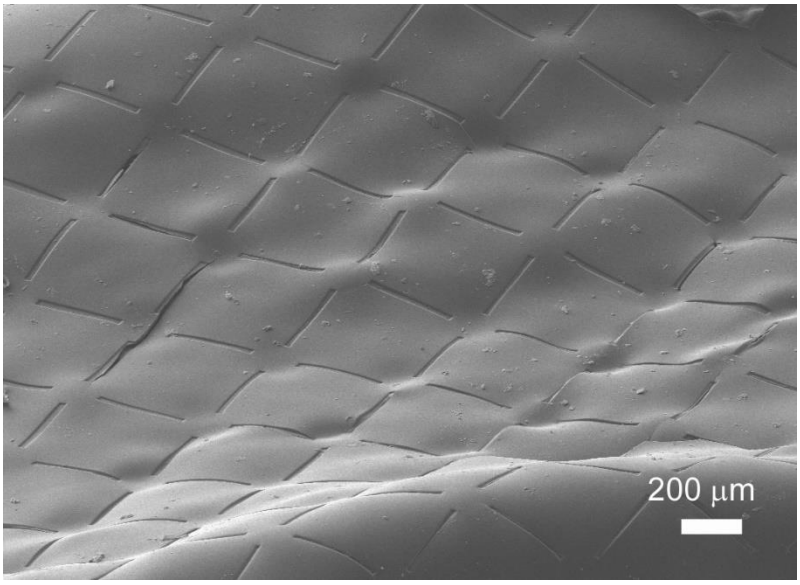

Figure S2 –By reducing the exposure time (in this experiment, the exposure time was 1 s), it is possible to engineer weak spots in the films in the form of unopened or partial cuts. This technique may be used to photolithographically form wrinkles in films.

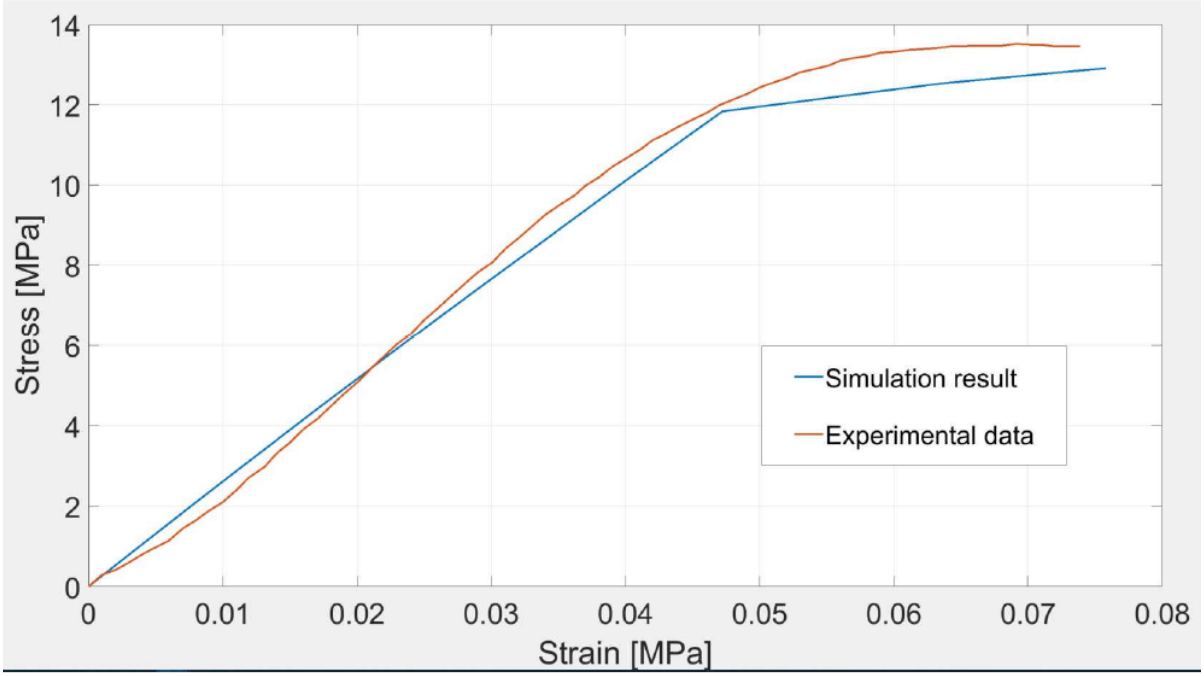

Simulation and comparison to a pristine film (no cuts).

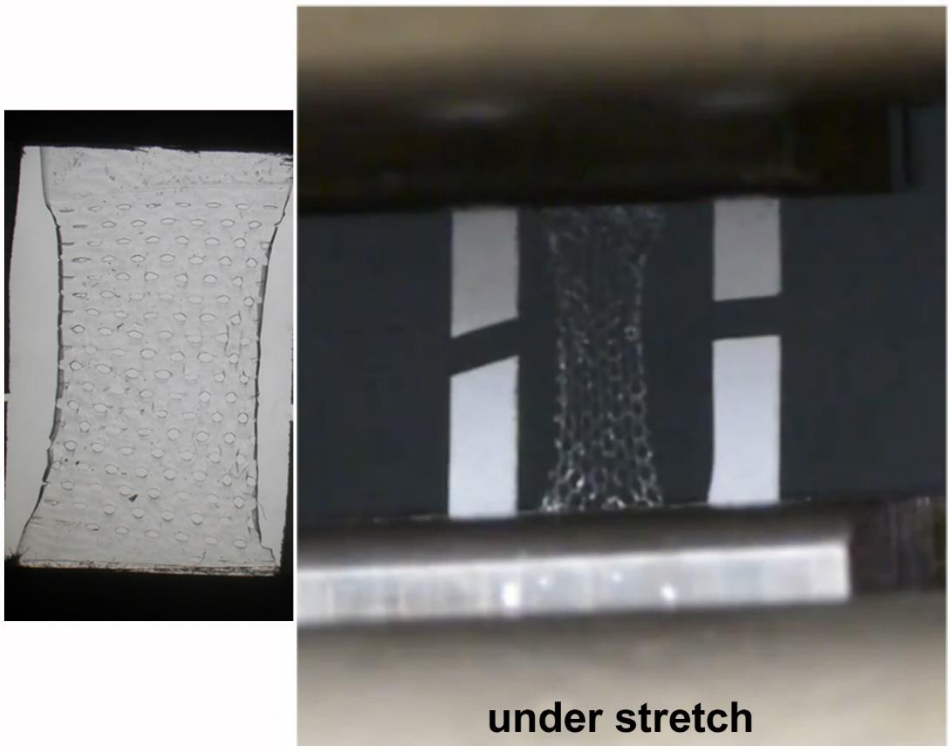

Figure S3 – Tensile testing of the kirigami films using a conventional tester. The films can be stretched to ~40 % strain without failure. In comparison, pristine films fail at 5-8% strain.

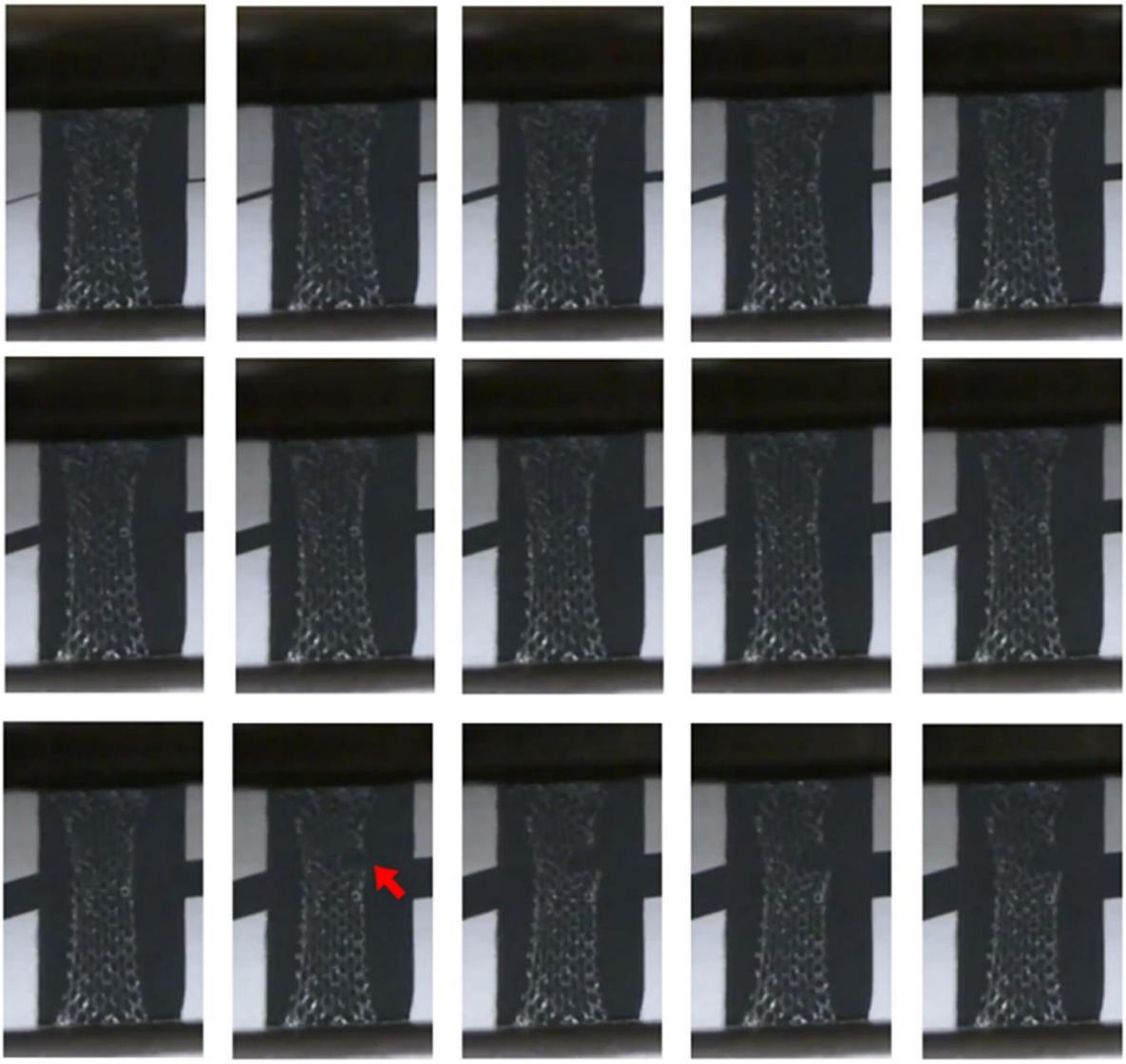

Figure S4 – Stills from video taken for kirigami stretch. The red-arrow in the bottom row indicates the point of failure of the film. The failure then propagates through the entire film. The tensile apparatus retreats prior to complete film breakage.

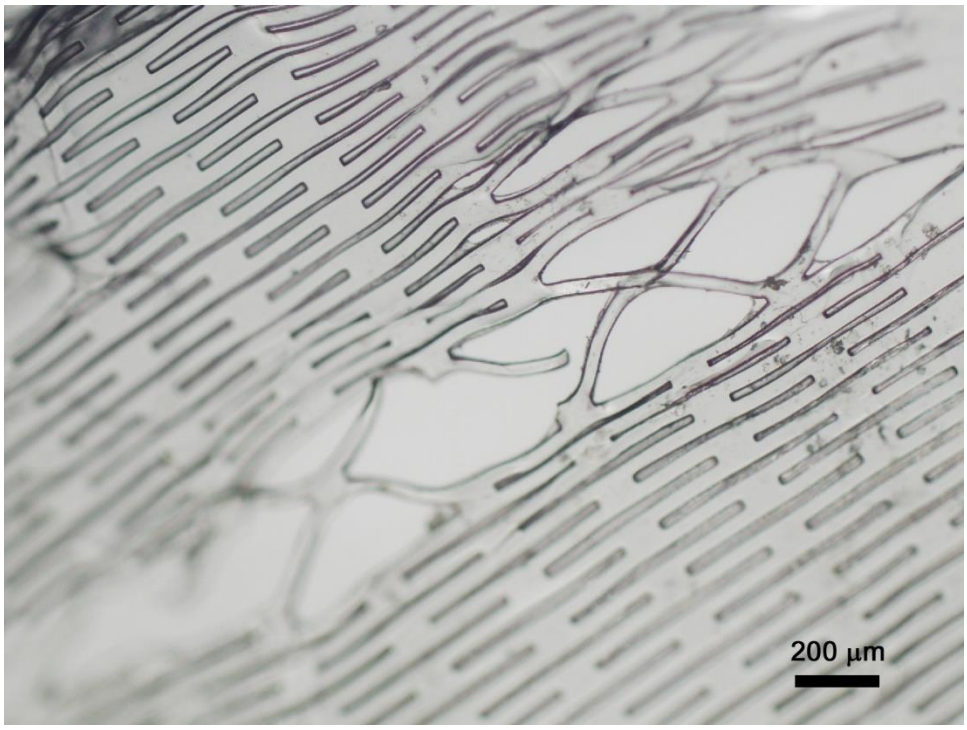

Figure S5 – Optical image showing one of the modes of failure on stretching a silk kirigami film with a slit geometry. Even though some of the cuts may tear, the entire structure does not come apart.

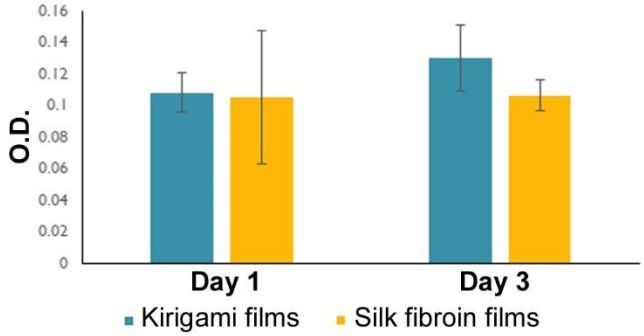

Figure S6: Cell viability. An MTT ((3-(4,5-Dimethylthiazol-2-yl)-2,5-diphenyltetrazolium bromide, a tetrazole) assay was conducted to determine the cell activity and viability. Human fibroblast cells were used and at least 4 replicates of each sample were measured. Following cell culture for 24 h, the cells were washed with 0.5 ml PBS and removed from the wash solution. 50 ul of MTT reagent (Abcam) were added and incubated at 37^{o}C for 3 hrs. After MTT Incubation, 150 µl of MTT solvent was added to elute the purple ice crystals of MTT and shaken for 15 min using an orbital shaker. 1.5 ml of DMSO was added to completely dissolve purple formazan. The absorbance was measured at 570 nm using a microplate reader and reported as O.D. in the figure. It can be seen that the presence of kirigami cuts did not negatively affect cell viability in comparison with standard fibroin film in the culture period considered. Note that the cell viability of silk fibroin films via MTT assays has been reported by other groups.[15-16]

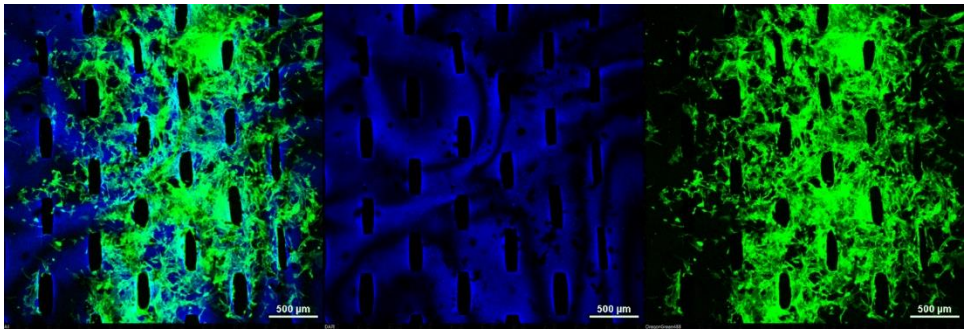

Attachment of C2C12 cells on the kirigami films preconditioned with expansion media.

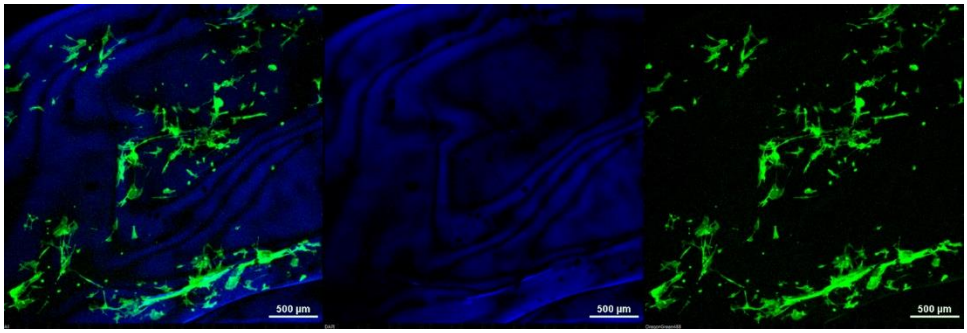

Control film (with no cuts) preconditioned with expansion media.

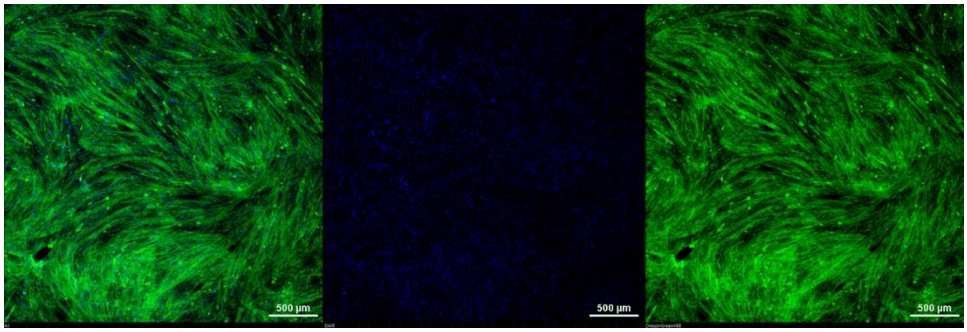

TCP control

Figure S7: Cell culture experiments on the silk kirigami films showing a) biocompatibility of the films, their robustness to cell sterilization protocols and b) the spreading of cells on the films.

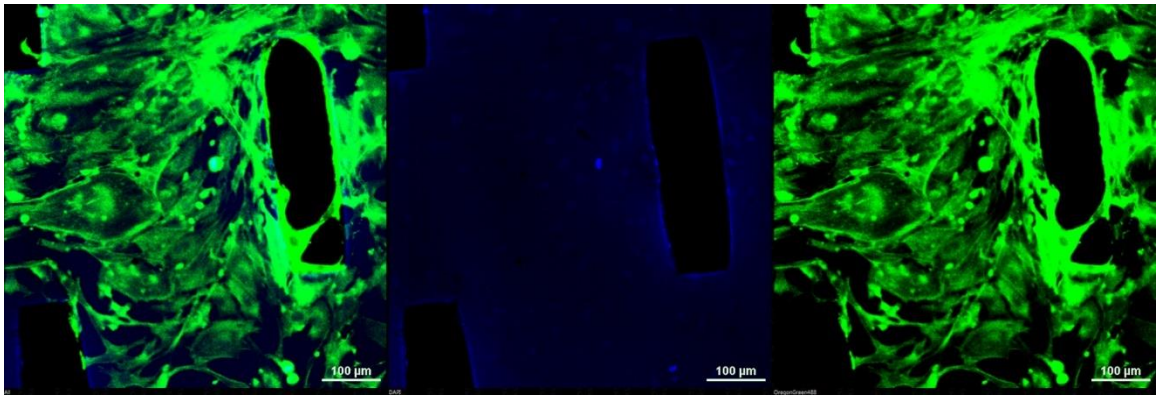

Figure S8 – Zoomed in image of a silk kirigami film that was pre-treated with fibronectin prior to attachment of C2C12 cells. Scale bar = 100 µm.

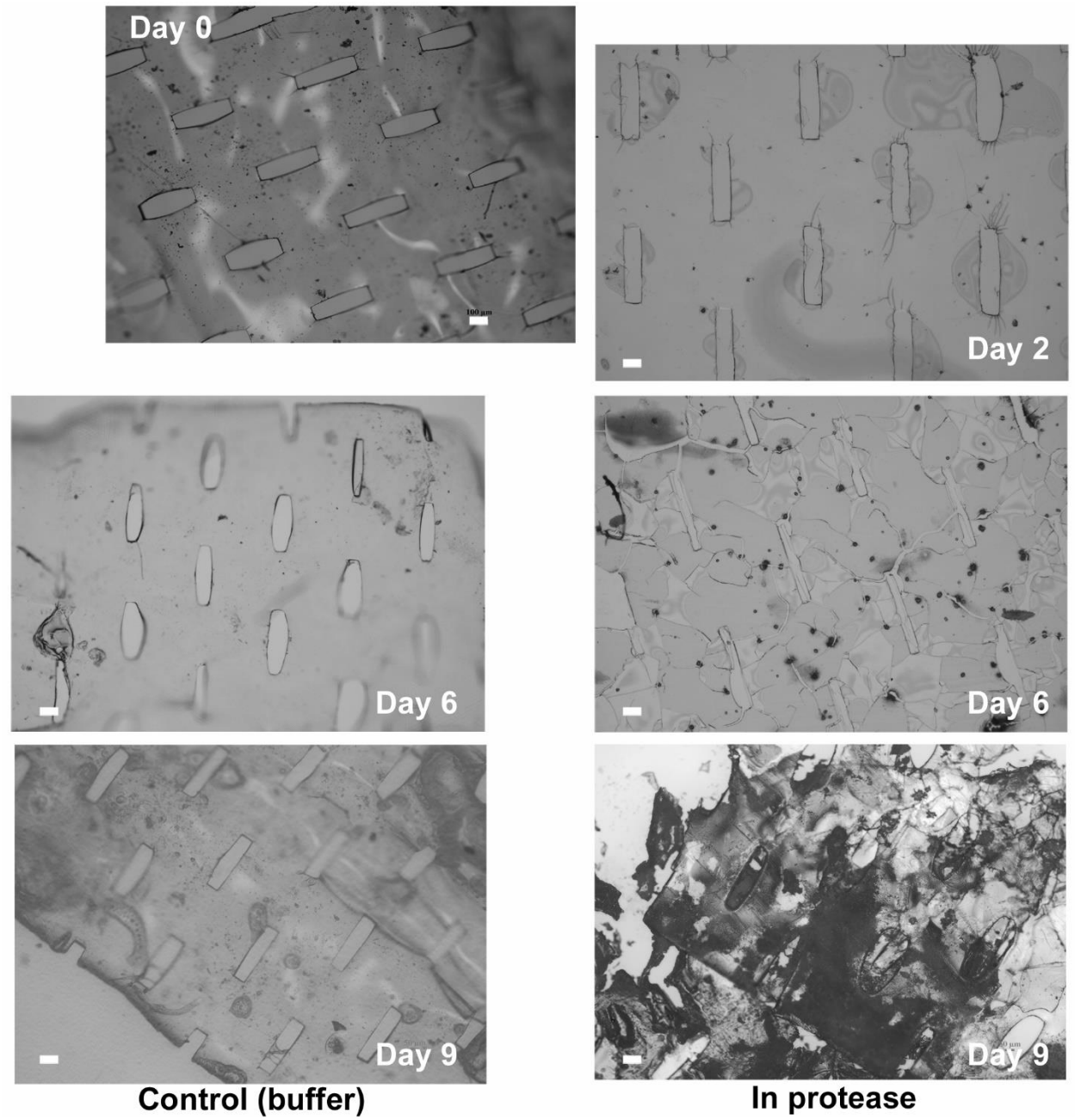

Figure S9 – Proteolytic degradation of silk kirigami sheets. On the left, films in (control) PBS buffer remain stable over several days (stored for a month with no loss in properties or morphology). On the right, a thin film (~10 μm) is completely biodegraded in solution of proteolytic enzyme (*protease XIV*), showing for the first time, a kirigami film that can be degraded. By controlling the thickness of the films, the rate of degradation can be controlled. Scale bar = 100 μm.

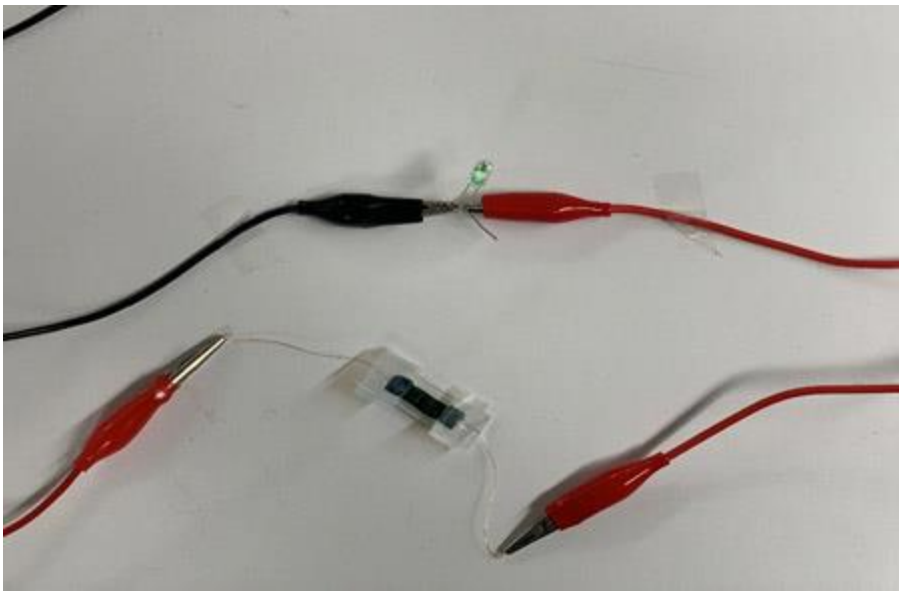

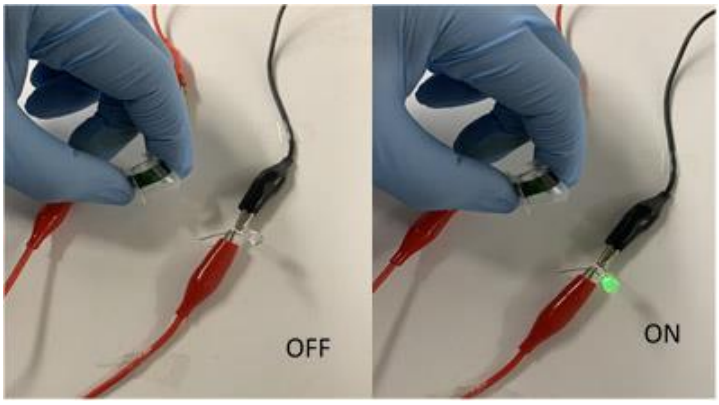

Figure S10 – Experimental set up to measure the properties of the silk kirigami films (11% PANI) under different bending conditions. The fibroin films containing PANI were developed in 1M LiCl/DMSO, and washed. The film was attached to a PDMS slab and wires were connected using carbon paste and epoxy. 100µL of PBS was dropcast on the films. Following a 5-minute incubation, the buffer was pipetted out. The film was subjected to bends of various radius of curvature and cyclic voltammetry was performed from -1 V to 1 V (results presented from -0.5V to 0.5 V).

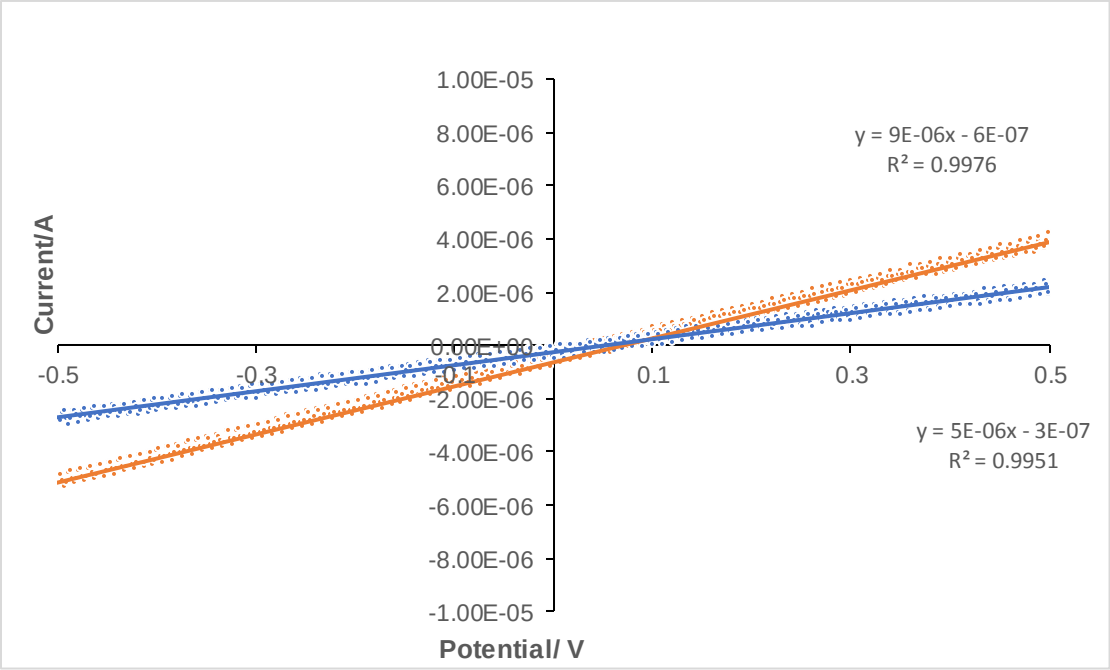

Figure S11 – Linear sweep voltammetry was taken under relaxed and stretched conditions. Films with 100 µm cuts (slit geometry – slit width 100 µm, length 500 µm, gap spacing – 500 µm and gap width 500 µm) unstretched (**orange line**) and with 10% linear strain (stretch – **blue line**). Conductance changes from 9 µS to 5 µS.

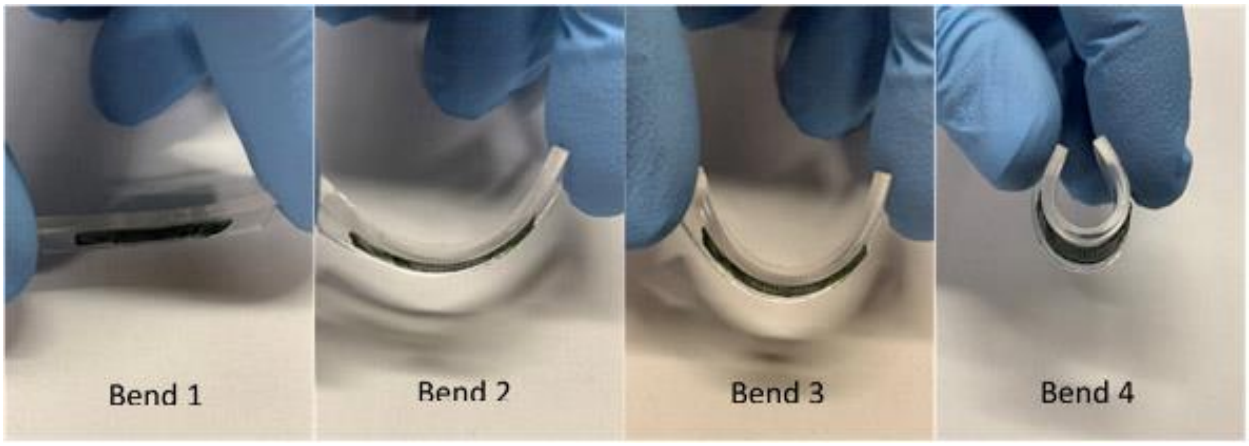

Figure S12 – Bending experiment corresponding to the data shown in Figure 4 of the manuscript. Bend 2 is 20^{o}, Bend 3 is 55^{o} (knee), Bend 4 is 180^{o}.

Theoretical model for the strength of silk kirigami films

d/2a / b/2a	**1.25**	**1.67**	**2.50**	+∞
2	0.4539	0.4174	0.2649	0.2030
4	0.1953	0.2408	0.1764	0.0743
6	0.0350	0.1182	0.1181	0.0349
8	-0.0953	0.0421	0.0735	0.0170
10	-0.1773	-0.0034	0.0508	0.0130
+∞	-0.5650	-0.2073	-0.0753	0

Table S2: Theoretical shielding factors for different kirigami patterns.

Simulation details:

The *commercial* software ABAQUS was used to compute the deformations of the kirigami films for three patterns (500 μm cuts, 1000 μm cuts and 'Y'-shaped or branched cuts).[17] The Python script contains three sections: mechanical and geometrical parameters, cut patterns and the constitutive model. The section "Mechanical and geometrical parameters" shows the units used in the model, and the values of the parameters used to perform a specific simulation: geometric parameters, mechanical properties of the material [Young's modulus E, Poisson's ratio v], mass density, and the loading condition of the sample (load or defect).

The geometry consists of three different parts, called "sketches" in ABAQUS. The "plateSketch" defines the part shape and dimensions, the "cutSketch" contains the pattern of the cuts, and the "partSketch" creates a domain partition to control the meshing algorithm. The mesh is composed of 6-node triangular thin shell elements (STRI65) near the cut tips to limit elements distortion upon cut opening, and 8-node quadrangular thin shells (S8R5) for the rest of the domain. To define the boundary conditions, we used a sub-set called "fixedEdge" containing the upper shell edge, whereas "movingEdge" contains the lower shell edge. The script proceeds to create cuts and partitions. The function "cut" takes the central point of the cut and cut type (i.e. horizontal, vertical or curvilinear) as input and adds the cut line to the "cutSketch" and four circles centered on the two cut tips (two each) to the "partSketch". Moreover, partitioning each cut in two halves

allows introducing a “defect” in correspondence of the middle point of each cut. This defect triggers the out-of-plane instability typical observed in kirigami structures.

The mechanical constitutive model is elastoplastic with isotropic linear elasticity and linear hardening. The material density is necessary since the buckling onset requires a dynamic analysis.

Finally, the “part” object collects all the geometrical and material parameters. This is translated in a physical domain by defining an “Instance” of “Assembly” in the ABAQUS language. Boundary conditions were set. The sub-domain “fixedEdge” is constrained, removing six degrees of freedom. During the first part of the simulation, the “movingEdge” was fixed, and one boundary condition for this subdomain was added.

Videos of the Simulations are included as separate files.

References:

1. Guan, Y.-S.; Zhang, Z.; Tang, Y.; Yin, J.; Ren, S., Kirigami-Inspired Nanoconfined Polymer Conducting Nanosheets with 2000% Stretchability. *Adv*. *Mater*. **2018,** *30*, 1706390.
2. Groeger, D.; #252; Steimle, r., LASEC: Instant Fabrication of Stretchable Circuits Using a Laser Cutter. In *Proceedings of the 2019 CHI Conference on Human Factors in Computing Systems*, ACM: Glasgow, Scotland UK, 2019;1-14.
3. Shyu, T. C.; Damasceno, P. F.; Dodd, P. M.; Lamoureux, A.; Xu, L.; Shlian, M.; Shtein, M.; Glotzer, S. C.; Kotov, N. A., A Kirigami Approach to Engineering Elasticity in Nanocomposites through Patterned Defects. *Nat*. *Mater*. **2015,** *14*, 785.
4. Xu, R.; Zverev, A.; Hung, A.; Shen, C.; Irie, L.; Ding, G.; Whitmeyer, M.; Ren, L.; Griffin, B.; Melcher, J.; Zheng, L.; Zang, X.; Sanghadasa, M.; Lin, L., Kirigami-inspired, Highly Stretchable Micro-supercapacitor Patches Fabricated by Laser Conversion and Cutting. *Microsyst*. *Nanoeng*. **2018,** *4*, 36.
5. Liu, Z.; Du, H.; Li, J.; Lu, L.; Li, Z.-Y.; Fang, N. X., Nano-kirigami with giant optical chirality. *Sci. Adv*. **2018,** *4*, eaat4436.
6. Blees, M. K.; Barnard, A. W.; Rose, P. A.; Roberts, S. P.; McGill, K. L.; Huang, P. Y.; Ruyack, A. R.; Kevek, J. W.; Kobrin, B.; Muller, D. A.; McEuen, P. L., Graphene kirigami. *Nature* **2015,** *524*, 204.
7. Lamoureux, A.; Lee, K.; Shlian, M.; Forrest, S. R.; Shtein, M., Dynamic Kirigami Structures for Integrated Solar Tracking. *Nat*. *Commun*. **2015,** *6*.
8. Yamamoto, Y.; Harada, S.; Yamamoto, D.; Honda, W.; Arie, T.; Akita, S.; Takei, K., Printed Multifunctional Flexible Device with an Integrated Motion Sensor for Health Care Monitoring. *Sci. Adv*. **2016,** *2*, e1601473.
9. Baldwin, A.; Meng, E., Kirigami Strain Sensors Microfabricated From Thin-Film Parylene C. *J. Microelectromech. Syst*. **2018,** *27*, 1082-1088.
10. Zheng, W.; Huang, W.; Gao, F.; Yang, H.; Dai, M.; Liu, G.; Yang, B.; Zhang, J.; Fu, Y. Q.; Chen, X.; Qiu, Y.; Jia, D.; Zhou, Y.; Hu, P., Kirigami-Inspired Highly Stretchable Nanoscale Devices Using Multidimensional Deformation of Monolayer MoS2. *Chem*. *Mater*. **2018,** *30*, 6063-6070.
11. Ma, R.; Wu, C.; Wang, Z. L.; Tsukruk, V. V., Pop-Up Conducting Large-Area Biographene Kirigami. *ACS Nano* **2018,** *12*, 9714-9720.

12. Bao, Y.; Hong, G.; Chen, Y.; Chen, J.; Chen, H.; Song, W.-L.; Fang, D., Customized Kirigami Electrodes for Flexible and Deformable Lithium-Ion Batteries. *ACS Appl. Mater. Interfaces* **2020,** *12*, 780-788.

13. Tang, Y.; Li, Y.; Hong, Y.; Yang, S.; Yin, J., Programmable Active Kirigami Metasheets with more Freedom of Actuation. *Proc. Natl. Acad. Sci. U.S.A.* **2019,** *116*, 26407.

14. Choi, G. P. T.; Dudte, L. H.; Mahadevan, L., Programming Shape using Kirigami Tessellations. *Nat. Mater.* **2019,** *18*, 999-1004.

15. Liu, T.-l.; Miao, J.-c.; Sheng, W.-h.; Xie, Y.-f.; Huang, Q.; Shan, Y.-b.; Yang, J.-c., Cytocompatibility of Regenerated Silk Fibroin Film: A Medical Biomaterial applicable to Wound Healing. *Journal of Zhejiang University SCIENCE B* **2010,** *11*, 10-16.

16. Panico, A.; Paladini, F.; Pollini, M., Development of Regenerative and Flexible Fibroin-based Wound Dressings. *J. Biomed. Mater. Res. Part B* **2019,** *107*, 7-18.

17. Barbieri, E.; Ongaro, F.; Pugno, N. M., A J-Integral-Based Arc-Length Solver for Brittle and Ductile Crack Propagation in Finite Deformation-Finite Strain Hyperelastic Solids with an application to Graphene Kirigami. *Computer Methods in Applied Mechanics and Engineering* **2017,** *315*, 713-743.